Earth System
Dynamics

Discussions

Open Access

1 **The "NorESM1-Happi" used for evaluating differences**

2 **between a global warming of 1.5°C and 2°C, and the role of**

3 **Arctic Amplification**

4 Trond Iversen[1,2], Ingo Bethke[3], Jens B. Debernard[1], Lise S. Graff[1], Øyvind Seland[1], Mats

5 Bentsen[3], Alf Kirkevåg[1], Camille Li[4], Dirk J. L. Olivié[1]

6 [1]Norwegian Meteorological Institute, P.O.Box 43, Blindern, 0313 Oslo, Norway

7 [2]Dep. of Geosciences, University of Oslo, P.O. Box 1047 Blindern, 0315 Oslo, Norway

8 [3]Uni Research Climate, Bjerknes Centre for Climate Research, P.O. Box 7810, 5020 Bergen, Norway

9 [4]Geophysical Institute, University of Bergen, Bjerknes Centre for Climate Research, P.O. Box 7803, 5020

10 Bergen, Norway

11 *Correspondence to:* T. Iversen (trond.iversen@met.no)

12

13 **Abstract.** The global NorESM1-M model that produced results for CMIP5 (http://cmip-

14 pcmdi.llnl.gov/cmip5/index.html) has been slightly upgraded to NorESM1-Happi, and has been run

15 with double resolution (~1° in the atmosphere and the land surface) to provide model simulations to

16 address the differences between a 1.5°C and a 2.0°C warmer climate than the 1850 pre-industrial. As a

17 part of the validation of temperature-targeted model simulations, the atmosphere and land models have

18 been run fully coupled with deep ocean and sea-ice as an extension of the NorESM1-M which

19 produced CMIP5-results. Selected results from a standard set of validation experiments are discussed:

20 a 500-year 1850 pre-industrial control run, three runs for the historical period 1850-2005, three

21 detection and attribution runs, and three future projection runs based on RCPs. NorESM1-Happi has a

22 better representation of sea-ice, improved Northern Hemisphere (NH) extratropical cyclone and

23 blocking activity, and a fair representation of the Madden-Julian oscillation. The amplitude of ENSO

24 signals is reduced and is too small, although the frequency is improved. The strength of the AMOC is

25 larger and probably too large. Modern era global near-surface temperatures and the cloudiness are

26 considerably under-estimated, while the precipitation and the intensity of the hydrological cycle are

27 over-estimated, although the atmospheric residence time of water-vapour appears satisfactory.

28 An ensemble of AMIP-type runs with prescribed SSTs and sea-ice from observations at present-day

29 and a set of global CMIP5 models for a 1.5°C and a 2.0°C world (i.e. AMIP) has been provided by the

30 model to a multi-model project (HAPPI, http://www.happimip.org/). This paper concentrates on the

31 results from the NorESM1-Happi AMIP runs, which are compared to results from a slab-ocean

Earth System
Dynamics
Discussions

1   version of the model (NorESM1-HappiSO) designed to emulate the AMIP simulation allowing SST

2   and sea-ice to respond. The paper discusses the Arctic Amplification of the global change signal. The

3   slab-ocean results generally show stronger response than the AMIP results to a global change, such as

4   reduced NH extratropical cyclone activity, and different changes in the occurrence of blocking. A

5   considerable difference in the reduction of sea-ice in the Arctic between a 1.5^{o}C and a 2.0^{o}C world is

6   simulated. Ice-free summer conditions in the Arctic is estimated to be very rare for the 1.5^{o}C case, but

7   to occur 40% of the time for the 2.0^{o}C case. These results agree with some fully coupled models, but

8   need to be further confirmed.

9

10   **1   Introduction**

11   In *The Paris Agreement*, the parties to the United Nations Framework Convention on Climate Change

12   (UNFCCC) have established a long-term temperature goal for climate protection of "holding the

13   increase in the global average temperature to well below 2°C above pre-industrial levels and pursuing

14   efforts to limit the temperature increase to 1.5^{o}C above pre-industrial levels, recognising that this

15   would significantly reduce the risks and impacts of climate change" (UNFCCC, 2015). This has

16   triggered considerable attention from climate modelling groups and researchers alike (e.g. Hulme,

17   2016; Peters, 2016; Rogelj and Knutti, 2016; Mitchell et al., 2016; Anderson and Nevins, 2016;

18   Boucher et al., 2016; Schleussner et al., 2016). For example, a special issue of the electronic journal

19   *Earth System Dynamics* focusing a 1.5^{o}C or a 2°C global warming compared to pre-industrial

20   conditions is underway. A Special Report that will discuss the differences in climate and climate

21   impacts   between   a   "1.5^{o}C   world"   and   a   "2.0^{o}C   world"   is   under   development

22   (http://www.ipcc.ch/report/sr15/), and results in the present paper and many other scientific articles are

23   intended to contribute to that report.

24   In addressing differences in impacts of the ceilings 1.5 and 2°C in global warming, there are two basic

25   weaknesses of available climate projections from the Coupled Model Intercomparison Project (CMIP)

26   as reported in the assessment reports from the Intergovernmental Panel for Climate Change (IPCC).

27   The body of research assessing impacts under a 1.5^{o}C world is small compared to higher emission

28   scenarios (James et al., 2017), and model simulations have been made on the basis of development

29   scenarios which give rise to a top of the model atmosphere (TOA) radiative forcing, rather than

30   selected temperature targets. New types of model calculations are therefore necessary to provide

31   support to the follow-up of The Paris Agreement (e.g. Mitchell et al., 2016). One example presented

32   by Sanderson, et al., (2017) is to develop a simple multi-parameter model which is designed to

33   emulate the model climate of a fully coupled climate model, and use this emulator to arrive at forcing

34   scenarios that produce developments towards a 1.5^{o}C and a 2°C global warming in equilibrium.

1   We have decided to follow the approach presented in Mitchell et al. (2017) under the acronym *HAPPI*

2   (Half a degree additional warming, prognosis and projected impacts, http://www.happimip.org/). The

3   main multi-model ensemble experiments for HAPPI are of the AMIP-type (Atmospheric Model Inter-

4   comparison Project) for the present-day situation and for possible future situations which target the

5   agreed global temperature ceilings (Mitchell et al., 2017; and http://www.happimip.org/). These

6   experiments are based on prescribed sea-surface temperatures (SST) and sea-ice, although the

7   employed atmosphere and land model components are taken from a fully coupled ESM. Papers

8   dealing with the main multi-model results and analyses of differences in climate-related impacts

9   between a 1.5°C and a 2.0°C warmer world (relative to the 1850 pre-industrial climate) from HAPPI,

10   are submitted to the mentioned special collection of papers in Earth System Dynamics (*The Earth*

11   *System at a global warming of 1.5°C and 2.0°C*).

12   The present paper documents a selection of major properties of the coupled Norwegian Earth System

13   Model dedicated for HAPPI (*NorESM1-Happi*). The model is a modified version of the NorESM1-M

14   (Bentsen et al., 2013; Iversen et al., 2013, Kirkevåg et al., 2013) used for the fifth cycle of CMIP

15   (CMIP5) and referred to in the fifth assessment report of IPCC (IPCC, 2013). By October 2017,

16   NorESM1-M has been referred to in almost 500 CMIP5-related publications (https://cmip-

17   publications.llnl.gov/search?type=model&option=NorESM1-M). The model is also equipped with a

18   thermodynamic slab ocean (SO) model (*NorESM1-HappiSO*). Throughout the paper, NorESM1 refers

19   to either of the two model versions, while the extensions -M and -Happi are used to specifically denote

20   one of them. Since Bentsen et al. (2013) and Iversen et al. (2013) presented, in great detail, the

21   NorESM1-M, this paper emphasizes selected properties of NorESM1-Happi and changes since

22   NorESM1-M.

23   The role of Arctic Amplification (AA) for a given level of global warming (Arrhenius, 1896; Manabe

24   and Stouffer, 1980, Holland and Bitz, 2003, Feldl et al., 2017) is relevant for the consequences of the

25   Paris agreement. The relevance of AA is first of all due to in-situ changes in the sea-ice and snow-

26   cover. In the next instance it can be relevant for the potential trigger of Arctic-specific irreversible

27   feedbacks, as well as the possible (but still controversial) changes in quasi-persistent mid-latitude

28   weather patterns due to reduced meridional temperature contrasts (Francis and Vavrus, 2012; Screen

29   and Simmonds, 2013; Cohen et al., 2014; Barnes and Polvani, 2015). Although the amplitude and

30   pattern of AA varies between models, it is nevertheless a robust response to a positive radiative

31   forcing predominantly driven by a positive regional lapse-rate feedback (negative at lower latitudes)

32   and a positive albedo feedback due to reduced sea-ice and snow-cover (Winton, 2006; Pithan and

33   Mauritsen, 2014). Even for the remote and regionally localized forcing caused by reduced European

34   sulphate aerosols since the 1980s, the AA has been calculated with a strong response (Acosta Navarro

35   et al., 2016).

Earth System
Dynamics

Discussions

1   We use the slab-ocean model (NorESM1-HappSO) to predominantly assess how the AA may differ

2   between equilibrated 1.5°C and 2°C global warming levels since the 1850 pre-industrial level. A

3   weakness of the AMIP-type approach of HAPPI is the enforcement of prescribed SST and sea-ice

4   fields. This leads to a pattern of AA which is basically pre-defined and does not belong to a natural

5   realization of the model-climate's SST and sea-ice. Representing the upper ocean as thermodynamic

6   slab with a fully dynamic sea-ice description attached to it, is not an ideal solution, but when it is

7   properly calibrated, it includes more degrees of freedom for the model when responding and

8   equilibrating with the forcing of the system. The reliability of the SO model results is higher if their

9   quality is approximately the same or better than the fully prescribed experiments.

10   The calibration of the SO model is tuned to fit the driving conditions for the HAPPI experiments

11   performed with NorESM1-Happi, but without prescribing the SST and sea-ice. The SO experiments

12   thus allow explicit feedback processes involving the SSTs and the sea-ice, but without calculation of

13   ocean currents. Further comparisons with results from the NorESM1-Happi coupled to the deep ocean

14   are done as well, although in that case without sufficient accounting for model uncertainties and

15   internal variability.

16   This paper first describes the ingredients of the NorESM1-Happi model in section 2 emphasizing the

17   changes since NorESM1-M, and the slab ocean version NorESM1-HappiSO in section 3. Section 4

18   presents and discusses the properties of NorESM1-Happi as a coupled climate model, while some

19   aspects of the 1.5°C and 2.0°C global temperature targets are discussed in Chapter 5, emphasizing

20   Arctic amplification, extratropical cyclone activity and blocking, and the fate of Arctic sea-ice. Some

21   conclusions are given towards the end.

22

2   The NorESM1-Happi model

24   This section reviews selected features of NorESM1, emphasizing own developed model processes and

25   differences between the model versions -M and -Happi. More complete descriptions of NorESM1-M,

26   and thus also most of NorESM1-Happi, are found in section 2 of Bentsen et al. (2013). NorESM1 is

27   based on the fourth version of the Community Climate System Model (CCSM4) developed in the

28   Community Earth System Model project at the US National Center for Atmospheric Research

29   (NCAR) in collaboration with many partners (Gent et al., 2011). Explicit description of the interactive

30   carbon cycle is not included, and the experiments employ prescribed concentrations of greenhouse

31   gases (GHG).

32   Changes in NorESM1-Happi compared to NorESM1-M were mainly developed in the project

33   ACCESS (Arctic Climate Change, Economy and Society) financed under the 7th Framework

34   Programme of the European Union (http://www.access-eu.org/). The modifications included double

1   horizontal resolution in the atmosphere and land model and a different tuning of the aging, and thus

2   albedo, of snow accumulated on sea-ice (Seland and Debernard, 2014). More recently an error in the

3   aerosol scheme (Kirkevåg et al., 2013) was found and rectified, resulting in faster condensation of

4   secondary gaseous matter on pre-existing particles.

5   ## 2.1   The Atmosphere

6   NorESM1's atmospheric component is based on the original CAM4 publicly released in April 2010

7   (Neale et al., 2010 and 2013). The finite volume dynamical core for transport calculations (Rasch et

8   al., 2006) is used. In NorESM1-Happi the horizontal resolution is 0.95^{o} latitude by 1.25^{o} longitude (in

9   short: 1° resolution), which is half the mesh-width used in NorESM1-M. In the vertical direction, 26

10   levels are used with a hybrid sigma-pressure co-ordinate and model top at 2.194 hPa.

11   In NorESM1 the atmospheric model (CAM4-Oslo) is extended by calculating online the lifecycles of a

12   range of natural and anthropogenic aerosol components from emissions and physico-chemical

13   processing in air and cloud droplets. The only prescribed aerosol concentrations are stratospheric

14   sulphate from explosive volcanoes in the historical period. Other aerosol components are

15   calculated from emissions. Correct modelling of forcing of anthropogenic aerosols depends

16   on the representation of natural background aerosols and the associated cloud droplet

17   properties (e.g. Hoose et al., 2009). Parameterization of aerosol interactions with the model's

18   schemes for radiation and warm cloud microphysics enable the calculation of direct and indirect

19   aerosol effects on climate (Kirkevåg et al., 2013). The model employs a prognostic calculation of

20   cloud droplet numbers using the Abdul-Razzak and Ghan (2000) scheme for condensation nuclei

21   activation, allowing for competition effects between aerosols of different hygroscopic property and

22   size.

23   The upper air burdens of aerosols and other atmospheric constituents exposed to precipitation

24   scavenging are sensitive to processes taking place in deep convective clouds (Seland et al., 2008). In

25   NorESM1 deep moist convection is parameterized as in CCSM4 by the scheme of Zhang and

26   McFarlane (1995), extended with plume dilution and convective momentum transport (Richter and

27   Rasch, 2008; Neale et al., 2008). Both Samset et al. (2013) and Allen and Landuyt (2014) indicated

28   that NorESM1-M had too high upper air concentrations of black carbon (BC) aerosols. This could

29   cause overestimated absorption of solar radiation, suppressed upper-level cloudiness, and exaggerated

30   static stability.

31   The physical properties of BC differ from other anthropogenic aerosols by its occurrence in

32   hydrophilic form after pyrolysis and inefficient combustion of fossil fuel. By mixing with hygroscopic

33   matter, BC aerosols become hydrophilic, and the efficiency of this BC aging reduces the ability of BC

1   to survive vertical transport in deep convective clouds (Allen and Landuyt, 2014). The increased

2   efficiency of aerosol condensation in NorESM1-Happi, enhanced the scavenging efficiency of BC

3   compared to NorESM1-M, and Fig. 1 shows considerably reduced atmospheric burdens of BC, in

4   particular in the middle layers of the free troposphere. Nevertheless, to the extent that the observed

5   vertical profile of BC during the HIPPO-campaign (Schwartz et al., 2013) is representative for the

6   vertical distribution of BC in general, the model still mixes the BC too high up, and the transport and

7   scavenging in deep convective clouds probably needs to be improved. Table 1 summarizes the global

8   budget for the aerosol particles and their precursors for NorESM1-Happi and NorESM1-M. All but

9   BC have minor changes in atmospheric burdens and residence times, while the reduction for BC is

10   substantial. It should be mentioned that a comprehensive discussion of the aerosols in NorESM is

11   underway in another publication.

12   ## 2.2   The Ocean

13   For NorESM1, the ocean model in CCSM4 is replaced by an elaborated version of the Miami

14   Isopycnic Community Ocean Model (MICOM) adapted for multi-century simulations in coupled

15   mode (Assmann et al., 2010; Otterå et al., 2010). The extensions of the ocean model since the original

16   MICOM are summarized by Bentsen et al. (2013) and include improved parameterization of diapycnal

17   mixing, thickness and isopycnal eddy diffusion, and the mixed layer depth. A grid with 1.125º

18   resolution along the equator is used with the Northern Hemisphere (NH) grid singularity located over

19   Greenland. The grid is a standard (gx1v6) provided by CCSM4, and the same ocean mask is used. The

20   bathymetry is created by averaging the depths of a high resolution data set (S2004; Marks and Smith,

21   2006) belonging to each ocean grid cell, and editing of the bathymetry is limited to setting key sills

22   and channels to their actual depths. A total of 53 model layers are used with layer reference potential

23   densities in the range 28.202–37.800 kg m^{-3}. Originally, MICOM has a single bulk surface mixed

24   layer. In NorESM1 the mixed layer is described by two model layers with freely evolving density. The

25   two layers are equally thick when the mixed layer is shallower than 20m, while the uppermost layer is

26   limited to 10m when the mixed layer is deeper than 20m.

27   In connection with the EU ACCESS project, external inertia-gravity waves were damped in shallow

28   regions in order to remove spurious oceanic variability in high latitude shelf regions. This damping is

29   kept in NorESM1-Happi.

30   ## 2.3   The Sea-Ice

31   *The sea ice model* in NorESM is the original CICE4 version used in CCSM4 (Gent et al., 2011;

32   Holland et al., 2012). The model employs the delta-Eddington short-wave radiation transfer (Briegleb

1   and Light, 2007), and parameterization of melt ponds and aerosols in snow and ice. The sea ice
2   component is configured on the same grid as the ocean component.

3   In NorESM1-Happi, wet snow albedo on sea-ice was decreased compared to NorESM1-M by
4   increasing the wet snow grain size and by allowing a more rapid metamorphosis from dry to wet snow.
5   This affects the Arctic sea-ice more than the Antarctic, since the latter is less frequently influenced by
6   mild and humid air.

7   As a result of the sea-ice albedo change and the reduced wave-induced oceanic variability along high-
8   latitude shelves, the large-scale distribution of sea-ice thickness across the Arctic was considerably
9   improved compared to NorESM1-M (Seland and Debernard, 2014; see also Fig. 11 below).

10 **2.4   The Land**

11 NorESM1 employs the original version 4 of the Community Land Model (CLM4) (Oleson et al.,
12 2010; Lawrence et al., 2011) of CCSM4, which included the SNow, ICe, and Aerosol Radiative model
13 (SNICAR; Flanner and Zender, 2006). The surface albedo and the vertical absorption profile depend
14 on solar zenith angle, albedo of the underlying snow, mass concentrations of atmospheric-deposited
15 aerosols, and ice effective grain size simulated with a separate snow aging routine. Atmospheric-
16 deposited aerosol components treated by SNICAR in NorESM1-Happi are black carbon and mineral
17 dust. In the experiments, the carbon–nitrogen (CN) cycle option of CLM4 is enabled (Thornton et al.,
18 2007; Gent et al., 2011), although their fluxes are diagnostically determined and do not influence other
19 model components. CLM4 employs the same horizontal grid as CAM4-Oslo, except for the river
20 transport model which is configured on its own grid with a horizontal resolution of 0.5°.

21 **2.5   The Coupler**

22 *CPL7* was developed specifically as a coupler for CCSM4 (Craig et al., 2012) and it is used in
23 NorESM1 without changes. It controls the exchange of information between model components and
24 the execution of the coupled system, by organizing the components of the coupled model into a single
25 executable, and issuing calls to initialization, run, and finalization routines for each model component.
26 The components can be configured to run sequentially, concurrently, or as a combination, thus
27 enabling optimal use of the hardware resources.

28 In NorESM1, fields and fluxes are exchanged between the components half-hourly, except for the
29 ocean components that are coupled once per day. The land and ice components are responsible for
30 computing the atmosphere/land and atmosphere/ice fluxes, respectively, while the coupler computes
31 the atmosphere/ocean fluxes every half hour, providing the instantaneous fluxes to the atmosphere and
32 daily mean fluxes to the ocean component.

Earth System
Dynamics
Discussions

1

2   ## 3   Emulating the oceanic response with a Slab Ocean (SO)

3   A slab ocean model (SO) has been set up for a specific purpose related to the design of the multi-

4   model experiments of the HAPPI-project (Mitchell et al., 2017; http://www.happimip.org/). Those

5   experiments are of the AMIP type, in which any change in the sea-surface temperature (SST) and sea-

6   ice cover are prescribed in combination with changes in the major elements producing radiative

7   forcing in the representative concentration pathways RCP2.6 and RCP4.5. Combinations of these

8   elements are constructed based on the CMIP5 multi-model ensemble in order to target the two

9   imagined future states defined by increase in global surface air temperature (SAT) above the 1850 pre-

10 industrial level: 1.5ºC and 2.0ºC. Even though the prescribed changes to future states are based on

11 fields from fully coupled model runs, the feedbacks behind amplification of climate change signals

12 will not be present in the HAPPI experiments. With NorESM1-HappiSO we intend to investigate if

13 this calculated amplification may depend on feedbacks that involve changes in Arctic sea-ice and SST

14 which are not present in the multi-model HAPPI experiments.

15 A slab ocean model does not calculate ocean circulation and associated fluxes, but treats the upper

16 ocean mixed layer as a single layer which buffers heat-fluxes through the ocean surface, i.e. a

17 thermodynamic "slab" governed by the equation

18
$$\rho_0 c_0 h_{mix} \frac{\partial SST}{\partial t} = F_{net} - Q_f \qquad (1)$$

19 where the thickness h_{mix} of the slab varies in space but not in time, ρ_0, and c_0, respectively, are the

20 density and heat capacity of the mixed layer sea-water, SST is the sea-surface temperature which in

21 this connection equals the mean, mixed-layer temperature. F_{net} is the net input of heat through the

22 ocean surface from the atmosphere and sea-ice, and Q_f is the net divergence of heat not accounted for

23 by the explicit processes needed to maintain a stable climate with a predefined geographical

24 distribution of SST.

25 The realism of the SO model climate depends on how Q_f is prescribed. In Bitz et al (2012), Q_f is

26 calculated using h_{mix}, SST, and F_{net} from a fully-coupled stable control simulation. Both h_{mix} and

27 SST should represent an assumed well-mixed layer in the vertical. With an annual mean (but still

28 spatially variable) mixed-layer thickness, it is quite straightforward to obtain balance with the annual

29 cycle of heat (Bitz et al., 2012). This method would give a SO model mean SST distribution very

30 similar to, and consistent with, the climate of the fully coupled model when external forcing is

31 unchanged. Here, this method has been used when estimating the equilibrium climate sensitivity

32 (ECS) for runs with abrupt CO_2 doubling ($\Delta T_{eq} = 3.31\ K$) and CO_2 quadrupling ($\Delta T_{eq4} = 6.74\ K$),

33 giving an average $\Delta T_{eq} = 3.34\ K$ for doubling of the atmospheric CO_2 –concentrations, Table 5). The

1   Q_f used in these experiments was diagnosed from the 1850 fully coupled pre-industrial control run

2   with NorESM1-Happi (Section 4.3), and kept constant in the different SO runs.

3   **3.1   Calibration of NorESM1-HappiSO experiments**

4   One drawback with this method for quantifying Q_f, is that biases in SST and the mean climate from

5   the fully coupled model are kept in the SO model, which makes comparison with the AMIP

6   experiments for HAPPI difficult. Therefore, as an alternative, we also use a restoring method similar

7   to Williams et al. (2001) and Knutson (2003), where a separate calibration run of the SO is done with

8   an additional restoring term $(SST - SST_{ext})/\tau$ added to the right-hand side of (1). SST_{ext} is an

9   externally imposed SST-field valid for some specific period (observation- or model-based) with τ as a

10   prescribed time-scale for adjustment. After this run, the new Q_f is defined by adding the monthly

11   climatology of the restoring flux to the Q_f used in the calibration run. Then, when used in a free SO

12   run (without restoring), the new Q_f ensures a modelled SST climate close to the SST_{ext} fields imposed

13   during the calibration. We have kept the sea-ice model free without any restoring or constraints to

14   observed fields during the calibration. This increases the realism of the ice-ocean heat fluxes going

15   into F_{net}, and ensures consistent changes in sea ice mass and energy. As in Bitz et al. (2012) the sea-

16   ice in the SO set-up employs the full CICE4 dynamic and thermodynamic model, which is the same as

17   used in the fully coupled NorESM1-M and NorESM1-Happi. However, some tuning of snow albedo

18   over sea ice have been done to increase the realism of sea ice extent under present day conditions

19   when using the restoring method for specifying Q_f.

20   In the present case, the purpose of the SO-model is to emulate regional patterns of the climate

21   response given a targeted ceiling for the global reference height temperature change relative to the pre-

22   industrial 1850 climate, taking into account the observed and analysed climate at present-day (2006-

23   2015). The experiments with NorESM1-HappiSO are designed to be directly comparable with the

24   AMIP-type runs with NorESM1-Happi for HAPPI, in which the SST and sea-ice are prescribed (see

25   Ch. 5). Three different calibrations of Q_f are therefore performed using the restoring method. For

26   present-day (PD) we use 10-year averaged SSTs determined by the observationally based *Operational*

27   *Sea Surface Temperature and Sea Ice Analysis* (OSTIA) for the decade 2006-2015 (Donlon et al.,

28   2012). In practice, this calibration also removes biases. For the future 1.5°C and 2.0°C climate scenario

29   states, we determine the Q_f which adjusts to the 10-year average SSTs used as input to the AMIP-type

30   HAPPI experiments. These were obtained by adding SST increments from the multi-model CMIP5

31   data to the OSTIA PD SST field. The different Q_f-fields thus emulate the effects of oceanic

32   circulation changes on the heat flux divergence in the well mixed layer.

1   The Q_f-fields are determined for each month of the year, and the values used in the slab ocean model

2   at a given grid-point and a given time is determined by linear interpolation between the former and the

3   next monthly value. The same Q_f-fields are used every year. Fig. 2 shows annual averages for the

4   present-day determined by the protocol for the HAPPI AMIP experiments (2006-2015) together with

5   the increments for the 1.5°C and the 2.0°C warmer world. In addition, we use the same CO_2-levels,

6   aerosols and precursor emissions, and other active forcing-agents as in the HAPPI AMIP experiments.

7   The Q_f for present-day (PD), which includes bias corrections, is dominated by large negative values

8   (hence SST increase) along the major currents in the North Pacific, North Atlantic, Southern Indian

9   Ocean, and the Atlantic sector or the Arctic. Positive values are mainly seen along the equator and in

10   some coastal upwelling zones. The increment patterns appear largely independent on the level of the

11   warming, with positive values (decreasing SST) over the Labrador Current, and negative values

12   (increasing SST) mainly in the tropics and north-west Pacific.

13

14   **4   Coupled Pre-industrial Control, Historical, and Projection Runs**

15   Throughout this paper, we use "piControl" to identify a 500-year control simulation with constant

16   external forcing prescribed for 1850 conditions. Aerosols and precursor emissions are as in Lamarque

17   et al. (2010). Emissions of sea-salt are calculated on-line according to surface wind speed and SST.

18   Concentrations of greenhouse gases (GHG) are consistent with preindustrial conditions in accordance

19   with CMIP5 (http://cmip-pcmdi.llnl.gov/cmip5/forcing.html). The incoming solar flux at the model

20   top is constant at 1360.9 W m^{-2} and the CO_2 mixing ratio is constant at 284.7 ppm.

21   Before the piControl, the 1° atmospheric and land resolution ACCESS version of the model (Seland

22   and Debernard, 2014) was spun up over 300 years starting from year 600 of the NorESM1-M spin-up

23   with 2° resolution atmosphere and land (Bentsen et al., 2013). The ocean and sea-ice were in both

24   cases run with 1° resolution. At year 900, the bug-fix for condensation in the aerosol-scheme was

25   introduced (see section 3.1), and the model was run for 500 years. These latter 500 years are

26   considered the piControl run for NorESM1-Happi, even though some adjustments over the first years

27   due to the aerosol fix should be expected. The aerosol fix is mainly affecting the upper air BC

28   concentrations (Table 1 and Fig. 1) with minor impacts on surface temperatures, surface energy fluxes,

29   and multi-decadal variability associated with the deep oceans (Sand et al., 2015; Stjern et al., 2017).

30   Three independent ensemble members to simulate the historical period from 1850 to 2015 were

31   branched off from the piControl at years 920 ("Hist1"), 950 ("Hist2") and 980 ("Hist3"). From 1850 to

32   2005 natural variations of solar radiation (Lean et al., 2005; Wang et al., 2005) and stratospheric

33   sulphate aerosol concentrations from explosive volcanoes (Ammann et al., 2003), as well as

34   anthropogenic GHG concentrations, aerosol emissions, and land-cover changes were prescribed using

Earth System
Dynamics
Discussions

1   the CMIP5 forcing-data (http://cmip-pcmdi.llnl.gov/cmip5/forcing.html). Forcing detection and

2   attribution experiments were run for the Hist1 experiment for "GHG only" (GHG=greenhouse gases),

3   "Aerosol only", and "Natural forcing only".

4   From 2005 onwards, the representative concentration pathway (RCP) scenarios (van Vuuren et al.,

5   2011) were the basis for a prolongation of Hist1 for climate projections until 2100. NorESM1-Happi

6   has run projections for RCP2.6, RCP4.5, and RCP8.5. The historical ensemble members were all

7   extended to 2015 using RCP8.5 for the years 2006-15.

4.1   Climate stability and present-day characteristics

9   NorESM1-Happi is a version of NorESM1-M with relatively minor updates. NorESM1-M is

10   thoroughly documented through CMIP5. The most radical change is the double horizontal resolution

11   in the atmosphere and land models. Many of the properties of NorESM1-Happi are therefore in reality

12   well documented. This paper presents selected major features only.

13   Fig. 3 shows the variation over the 500-year control period of selected key variables for the long-term

14   stability of the global climate, and Table 2 compares average values from Hist1 for 1976-2005 with

15   relevant observation and re-analyses. These can be compared with Fig. 2 and Table 1 in Bentsen et al.

16   (2013). Linear trends are estimated by linear regression of annual averages, and the statistical

17   significance of trends investigated by a t-test after adjusting the degree of freedom to account for

18   autocorrelation (Bretherton et al., 1999). A value of $p < 0.05$ is assumed to indicate that a non-zero

19   linear trend is statistically significant.

20   In the following we compare numbers from NorESM1-Happi with *numbers from NorESM1-M given*

21   *in brackets*, unless otherwise indicated. The global 500-year mean net radiation at the top of the model

22   atmosphere (TOA) is -0.042 Wm^{-2}, well below the desired range of ± 0.1 W m^{-2}. The linear 500-year

23   trend is +0.001 W m^{-2}, and is not statistically significant. The NorESM1-M value was +0.043 W m^{-2}

24   (the value +0.086 W m^{-2} reported in Bentsen et al. (2013) was inaccurately calculated). The flux

25   imbalance at the TOA causes a small sustained cooling of the earth system, as opposed to a warming

26   in NorESM1-M. The corresponding net heat flux into the ocean is +0.004 W m^{-2} (+0.122 W m^{-2}) with

27   a statistically insignificant linear trend of +0.004 W m^{-2} (-0.019 W m^{-2}). This tiny heat-flux causes the

28   global mean ocean temperature of 3.78^{o}C (3.81^{o}C) to increase by +0.008 K (+0.126 K) over 500 years,

29   which is statistically significant. A slow but statistically significant freshening of the ocean water

30   masses occurs over the 500 years, as the average ocean salinity of 34.72 g kg^{-1} (in both models) has a

31   negative change of 3.20 10^{-4} g kg^{-1} (3.14 10^{-4} g kg^{-1}). Fig. 4 shows that the salinity probably is

32   generally underestimated in the upper km of the ocean and overestimated below, while the trend is

33   hardly visible, as opposed to the results for NorESM1-M (Fig. 3 in Bentsen et al., 2013). The sea-

1   surface salinity (SSS) has an average global value of 34.57 g kg^{-1} (35.49 g kg^{-1}) with a small and

2   statistically significant positive (p=0.03) 500-year change of +0.005 g kg^{-1}.

3   In general, the piControl of NorESM1-Happi appears to be more stable and with smaller deviations

4   from the World Ocean Atlas of 2009 than NorESM1-M (compare Fig. 4 with Fig. 3 in Bentsen et al.,

5   2013). However, this long-term stability may to some extent be a consequence of an even stronger

6   Atlantic Meridional Overturning Circulation (AMOC) than in NorESM1-M. The 500-year average is

7   32.4 Sv (30.8 Sv) with a considerable and statistically significant positive 500-year increase of 1.0 Sv

8   (-0.6 Sv). As discussed in Iversen et al. (2013), a strong AMOC efficiently mixes heat into the deep

9   ocean, leaving less for surface heating and evaporation. The transport through the Drake Passage is

10   also larger in NorESM1-Happi than in NorESM1-M in the 1850 control run (135 Sv vs. 130 Sv), but

11   both models produce a statistically significant 500-year change (-6.98 Sv vs. -6.29 Sv).

12   The heat lost through the TOA and into the ocean from remaining parts of the climate system, i.e. the

13   atmosphere, the land surface, and the sea-ice, is 0.045 W m^{-2} (0.043 W m^{-2} for NorESM1-M), and is

14   comparable to the 1 degree version of CCSM4 which had a stronger negative TOA radiative heat

15   balance and also a negative heat flux at the ocean surface. The pre-industrial global near surface air

16   temperature of NorESM1-Happi is 12.74°C with a statistically significant (p=0.04) cooling of 0.032 K

17   over the 500 years. In comparison, NorESM1-M produced a 0.39 K higher pre-industrial near-surface

18   temperature with a statistically significant 500-year warming of 0.037 K. The average global sea-

19   surface temperature (SST) of 17.37°C (17.68°C) has a statistically insignificant 500-year decrease of

20   0.021 K (+0.03 K increase).

21   The pre-industrial temperatures are by construction supposed to be valid for a postulated stable climate

22   at 1850, and cannot adequately be compared to observations. Instead, the climate simulated with the

23   Hist-experiments for a recent 30-year period, e.g. 1976-2005, should be comparable to observationally

24   based data, see Tables 2, 3, 4, and column no. 3 from the right in Table 6. Both NorESM1 versions

25   produce a cold bias averaged over the global continents, but the negative bias is 0.52 K larger in

26   NorESM1-Happi (Table 3). Similarly, the negative SST bias is 0.31 K larger in NorESM1-Happi. This

27   larger bias is likely associated with higher horizontal resolution, in agreement with the experience

28   from the CCSM4-model (Gent et al., 2011). The cloud and precipitation parameterizations in CAM4

29   (the atmospheric model in CCSM4) and in CAM4-Oslo (used with NorESM1) tend to reduce the

30   cloud cover as grid resolution increases, and the ground surface loses more heat in the 1 degree

31   version than in the 2 degree version. This is corroborated by the numbers in Table 2 for both

32   NorESM1 versions, even though the net cloud radiative forcing itself is slightly less negative in

33   NorESM1-Happi, contributing to a warming compared to NorESM1-M. Other differences between the

34   models may also contribute, such as reduced absorption of solar radiation in clear air due to smaller

35   atmospheric burdens of BC, but this effect is masked by the effects of reduced cloud cover in

Earth System
Dynamics
Discussions

1   NorESM1-Happi. More short-wave (SW) radiation is absorbed by the ground surface, which
2   predominantly increase the latent heat flux by 2 W m^{-2} (Table 2). Furthermore, while the net radiative
3   imbalance at the TOA (ca. +0.5 W m^{-2}, see Fig. 5) is similar in the two model versions, the larger TOA
4   influx of SW radiation in NorESM1-Happi is almost entirely compensated by increased TOA outgoing
5   LW radiation, and more than 20% of this increase is from the clear sky.

6   Fig. 5 shows the calculated time-developments from 1850 to 2100 of some of the quantities on Table
7   2, without the adjustment due to the model top being slightly lower than the TOA seen from satellites,
8   including the three RCP-driven climate projections from 2005 to 2100. Curves for NorESM1-M are
9   included for reference. NorESM1-Happi experience a higher SW and LW heat fluxes at TOA, but the
10 net radiative imbalance in the two models is almost identical from 1850 to 2100. Nevertheless, the
11 global mean 2m-temperature is lower by ~0.3 K in NorESM1-Happi, yet the modelled global
12 precipitation rate is higher by ca. 0.05 mm d^{-1} (Table 3), which is consistent with the higher latent heat
13 flux (Table 2).

14 The budgets in the third column from the right in Table 6 can be compared to a corresponding column
15 in Table 5 from Iversen et al. (2013). While ca. 10 units (1 unit = 10^3 km^3 yr^{-1}) of water vapour are
16 evaporated from the oceans in NorESM1-Happi, the model difference in evaporation minus
17 precipitation (E-P) integrated over the world oceans is considerably smaller. Ca 80% of the added
18 oceanic evaporation is thus re-cycled back to the oceans. This cools and increases the salinity of the
19 upper ocean waters where the evaporation increase is large, which may contribute to the thermohaline
20 forcing and the strength of the AMOC. However, this effect is also influenced by the patterns of the
21 increased precipitation over ocean. Only 2 more units of water vapour are estimated to be transported
22 from the oceans to the continents in NorESM1-Happi, which are returned to the ocean as increased
23 river run-off. These 2 units add to 3 more which are recycled from continental evaporation, and thus
24 there are 5 more units of precipitation over continents in NorESM1-Happi than in NorESM1-M. In
25 summary, NorESM1-Happi has a slightly faster cycling of fresh water than NorESM1-M. The positive
26 biases diagnosed by comparing with GPCP-data in Table 3 indicate, however, that it may be too fast in
27 both models. The reason for these biases can be associated with the underestimated cloud cover, which
28 allows more direct sunlight to reach the ground than in reality. The cold bias in the lower atmosphere
29 still reduces the ability of the model atmosphere to keep the water vapour in the air, thus the efficient
30 recycling both over oceans and over continents.

31 Fig. 6 shows the global average 2m temperature relative to the 1851-1980 average for the Hist-
32 ensemble prolonged to 2015 with NorESM1-Happi, compared to the observationally based global
33 time-series from NASA-GISS (Hansen et al., 2010). Although the model slightly underestimates the
34 temperature maximum around 1950, there is good agreement after 1950. The calculated continental
35 2m temperatures are compared to the observationally based map from Climate Research Unit

1   (Mitchell and Jones. 2005). Except for in Europe and western parts of Asia, there is a widespread

2   under-estimate, hence the cold model bias. Fig. 7 compares the model-calculated fluxes of sensible

3   and latent heat with the FLUXNET Model Tree Ensembles (MTE) estimates (Jung et al., 2011), which

4   are restricted to vegetated land surface. It is striking that the sensible heat generally is too small, while

5   the latent heat, and thus the evaporation, is largely over-estimated at low latitude continents,

6   corroborating the argument about the low cloudiness allowing more solar radiation to reach the ground

7   and thus cause evaporation. The maxima in overestimations in Africa, America and Australia are

8   reduced relative to NorESM1-M, but there are increases in southern Europa and western parts of Asia.

9   The differences for sensible heat are very minor.

10   Fig. 8 shows evaluations of SST and SSS. The cold bias dominates the pictures also over oceans,

11   although there are exceptions along the SH storm-belt and in north-west and south-east Atlantic

12   Ocean. The amplitude of the positive biases is reduced in NorESM1-Happi compared to NorESM1-M

13   (Fig 12b in Bentsen et al., 2013), while the negative biases are almost the same. Hence the larger

14   underestimate of the global average (Table 3). The pattern of SSS-biases is almost the same as for

15   NorESM1-M (Fig 12c in Bentsen et al, 2013). SSS is considerably over-estimated at high latitudes in

16   the NH, while in the tropics and sub-tropics it is under-estimated.

17   The modelled and observed sea-ice extent for the recent few decades listed in Table 4, indicate

18   reduced biases in the simulation results from NorESM1-Happi compared to NorESM1-M, except for

19   the SH September maximum where the bias are larger. The variability in the data is represented with

20   the standard deviation, which is generally smaller or equal to the model biases. Both models have

21   positive biases except during the NH March maximum when the sea-ice cover is under-estimated,

22   mostly due to too little ice in the Labrador Sea (Fig. 9). The thickness of the sea-ice is shown together

23   with the extension in Fig. 9. The distribution of the Arctic sea-ice thickness is considerably improved

24   in NorESM1-Happi, with a pronounced cross-polar gradient with maximum thickness on the

25   Greenland-Canadian side (approaching 4 m) and a minimum along the Siberian coast. This

26   improvement was already mentioned in Seland and Debernard (2014).

27   Table 3 clearly documents that cloud cover is under-estimated in both NorESM1 versions, and that the

28   negative bias is increased to ca. 20% cloud cover units (the relative error is approximately 33%) with

29   the 1 degree version of NorESM1-Happi. The zonal averages in Fig. 10 show that the bias exists at all

30   latitudes, except close to the South Pole where the bias is positive. There are also too much low clouds

31   and fog in the winter Arctic atmosphere (not shown), which is a persistent problem in many climate

32   models, including the CCSM4 (Gent et al., 2011). The underestimated cloudiness is to some extent

33   compensated by exaggerated liquid water contents in the clouds, making them more opaque w.r.t.

34   radiation, except in the sub-tropics. Notice, however, that the values for liquid water path in Fig. 10b

35   are valid over oceans only, and the exaggeration is particularly pronounced over the marine

1   extratropical cyclone regions as discussed by Jiang et al. (2012). The zonally averaged precipitation

2   rate for winter and summer indicate good agreement with the Legates data (Legates and Willmott,

3   1990) in the tropics and with the GPCP (Global Precipitation Climatology Project, Adler et al., 2003)

4   elsewhere. The overestimates shown in Table 3 seem to originate in the tropics.

5   In summary, by the end of the 20th century the near-surface air temperature is simulated too

6   low by about 1.1-1.2 K (0.8-0.9 K in NorESM1-M) globally and 1.4-1.5 K (1.1-1.2 K) over

7   land. The global precipitation is estimated to be up to about 0.2 mm day^{-1} (0.15 mm day^{-1}) too

8   high, the evaporation from oceans is over-estimated by ca. 6% (4%), and the net flux between

9   oceans and continents are ca 12% (8%) over-estimated. The intensity of the water-cycle is

10   therefore even more overestimated in NorESM1-Happi than in NorESM1-M. Still, the

11   deduced atmospheric lifetime of water vapour is close to estimates based on Trenberth et al.

12   (2011), since fraction (E-P)/E over the oceans, which defines the fraction of oceanic

13   evaporation which is transported and precipitated over continents, is only 0.6% larger than

14   numbers from Trenberth et al. (2011). It has to be stressed that the model's faster hydrological

15   cycle is linked to increased lengths and areas of dry spells, due to the coupling between

16   precipitation and release of latent heat in the atmosphere which produces a positive feedback

17   with the vertical atmospheric circulation.

18   In order to attribute climate change and variability since 1850 to possible causes, a standard

19   set of single forcing simulations are made. In "GHG only", all but the prescribed greenhouse

20   gas concentrations are kept constant at the 1850-level; in "Aerosol only" all but aerosol

21   emissions are as in 1850; and in "Natural forcing only", only the natural contributions to the

22   forcing are varied after 1850. Figure 11 shows results for the global reference height air

23   temperature and for precipitation. The simulated warming since the 1970s can hardly be

24   reproduced with natural forcing only, and the greenhouse gases alone would lead to an

25   exaggerated warming since aerosols significantly dampen the warming. The signals for global

26   precipitation are less clear, even though they follow those for temperature. As discussed in

27   Iversen et al. (2013) the regional variations in the simulated precipitation changes are crucial,

28   since a more intense hydrological cycle in a warmer climate also leads to reduced annual

29   precipitation and more droughts in some regions while the precipitation intensity increases

30   (Giorgi et al. 2011). Iversen et al. (2013) discussed this in more detail.

Earth System
Dynamics
Discussions

4.2   Simulated variability and patterns

There are many patterns of variability of importance for the earth's climate and associated weather. Here we select to summarize the diagnosis of a few which are important for the NH, either directly or through apparent teleconnections. The present analysis is not meant to be complete.

The *Madden–Julian oscillation (MJO)* is the dominant mode of 30–90 days variability in the tropical atmosphere (Madden and Julian, 1971; Zhang, 2005) characterized by large-scale regions of enhanced and suppressed convection that propagate slowly eastward along the equator. The MJO interacts with several large-scale climate phenomena including ENSO (Hendon et al., 2007), and potentially extratropical variability and the North Atlantic Oscillation (NAO) (Cassou, 2008). The CCSM4 was one of the first global climate model that had a fair representation of MJO (Subramanian et al., 2011), and this was also the case in NorESM1-M (Bentsen et al., 2013). Fig. 12 shows the wavenumber–frequency spectra for the NH winter for the equatorial 850 hPa zonal wind U compared to ERA-Interim, and the outgoing longwave radiation (OLR) compared to NOAA satellite data. Although the model has too much energy on shorter periods than a month, the dominant maximum is between 40 and 60 days for wavenumber 1. The spectra are improved compared to NorESM1-M, in particular for OLR.

Extratropical cyclones are important vehicles for the atmospheric meridional transport of heat, humidity and momentum between the low and high latitudes, as well as the maintenance of the jet-streams themselves (e.g. Bratseth, 2001; 2003). *Persistent blocking* of eastward propagating cyclones can be important for the occurrence of droughts. The climatological storminess in the NH extratropics is diagnosed by taking the standard deviation of band-pass filtered 500 hPa geopotential height over 2.5 – 6 days (Blackmon, 1976). We refer to the patterns diagnosed in this way as a measure of *extratropical cyclone activity*, even though propagating ridges are included in the variability. Figure 13 shows the evaluation of the seasonal cyclone activity in the Hist-ensembles for 1976-2005 of NorESM1-Happi and NorESM1-M by comparison with the diagnoses of the ERA-Interim data for 1979-2008 (Dee et al., 2011). The cyclone activity is clearly under-estimated in all seasons in both model versions. However, the bias is considerably reduced in NorESM1-Happi, in particular over the Pacific Ocean in all seasons. Reduced bias is also seen where the Atlantic storm-tracks extends into the Nordic sea towards the Arctic, which is important for the weather and precipitation distribution in Europe. The under-estimate over the North Atlantic during winter is, however, considerable also in NorESM1-Happi. We believe most of the improvements in NorESM1-Happi can be ascribed to higher spatial resolution (e.g. Jung et al., 2012), and that the general under-estimated cyclone activity indicates that better resolution is needed in climate models.

1   *Extratropical blocking* is closely connected with persistent anticyclones, which can suppress

2   precipitation at mid-latitudes for periods of up to several weeks. The ability of climate models

3   to simulate and project the climatic occurrence of droughts in mid-latitudes is conditioned by

4   their ability to simulate blocking. We use the same index as in Iversen et al. (2013) to identify

5   NH extratropical blocking events. The TM-index (Tibaldi and Molteni, 1990) uses a

6   persistent reversal of the meridional gradient of the 500 hPa geopotential height around 50°N

7   as an indicator. Persistence was of at least 5 days was required and the reversed flow had to

8   be present at 7.5 degrees consecutive longitudes. Pelly and Hoskins (2003) relaxed the

9   requirement of predefined central blocking latitudes in order to reduce spurious detection. The

10 vTM index thus allows the central latitude to vary with the longitude of the climatological

11 storm track, by defining the central latitude where the maximum of the standard deviation of

12 the 2.5-6 days band-pass filtered geopotential height anomalies at 500 hPa are found. To

13 account for the seasonal cycle of the cyclone activity, the central latitude for a given month is

14 calculated as the climatological 3-month moving average centred on the given month.

15 Fig. 14 shows the seasonal blocking frequency for the Hist-ensemble of NorESM1-Happi and

16 NorESM1-M simulation for 1976-2005 compared to the ERA-Interim reanalysis for 1979-

17 2008 (Dee et al., 2011). NorESM1-Happi shows better results than NorESM1-M, although

18 important systematic errors still persists in several sectors and seasons. Best results are seen in

19 the autumn (SON), when the occurrence is close to perfect all places except for an under-

20 estimate in Atlantic Ocean. The errors are also smaller during spring (MAM), while in winter

21 the systematic under-estimate in the Atlantic-European sector is only slightly reduced. The

22 results are better over Europe in summer (JJA), but blocking over central Eurasia is under-

23 estimated and over-estimated in the Pacific sector. As discussed in Iversen et al. (2013), poor

24 model resolution seems to cause systematic errors of blocking occurrence.

25 *The El Niño–Southern Oscillation (ENSO)* is a dynamical feature that involves the ocean–atmosphere

26 interactions with major impacts on the climate variability of the tropical Pacific on seasonal to inter-

27 annual timescales (Wallace et al., 1998), and with a strong association to global scale patterns and

28 interaction (Trenberth et al., 1998; Straus and Shukla, 2002). NorESM1-M was amongst 9 out of 20

29 CMIP5 models that described both modes of the ENSO variability over the central and eastern tropical

30 Pacific Ocean (Kim and Yu, 2012). As in Bentsen et al., (2013), we use the de-trended monthly SST

31 anomalies of the NINO3.4 region (5°S - 5°N; 170°W - 120°W) to identify ENSO variability. The

32 NINO3.4 index is obtained by normalizing these SST anomalies by their long-term standard deviation.

33 Fig. 15 shows time series of the NINO3.4 index for the HadISST data set and for Hist1 of NorESM1-

1   Happi for the years 1900–2005. Also shown are SST anomalies from the corresponding years of the

2   1850 piControl. The standard deviation of NorESM1-Happi Hist1 and piControl are 0.55 K (0.92 K)

3   and 0.63 (0.86 K) respectively, where the numbers in brackets are for NorESM1-M. While both

4   numbers were larger than for HadISST (0.75 K) in NorESM1-M, they are now smaller for NorESM1-

5   Happi. The frequency of the ENSO variability is reduced in NorESM1-Happi and closer to the

6   HadISST, as a sharp peak in the frequency spectrum for NorESM1-M for 3 years periods was not

7   present for NorESM1-Happi (not shown).

8   ### 4.3   Climate sensitivity and Climate Projections

9   A basic reason for developing global earth system and climate models is for estimating the possible

10   impact of changes in external forcing on the climate. One single quantity is often referred to in order

11   to describe to what extent the climate responds to changes that leads to a radiative forcing, the climate

12   sensitivity. Most measures of climate sensitivity are single numbers that give the response of the

13   global near-surface air temperature to a standard specified TOA radiative forcing. Here we use

14   standard protocols from CMIP5 also adopted as in CMIP-DECK for qualifying a model for CMIP6

15   (Eyring et al., 2016). Two 150-year long runs with NorESM1-Happi start in year 920 of the piControl,

16   the same start year as Hist1. The "abrupt 4xCO$_2$" (quadrupling of atmospheric CO$_2$ concentrations at

17   t=0) is used to quantify the equilibrium climate sensitivity (ECS), and the "gradual 4xCO$_2$" (1%

18   increase per year until quadrupling) is used to quantify the transient climate response (TCR).

19   To calculate the ECS from first principles requires a full climate model run over several thousand

20   years (Boer and Yu, 2003). ECS is therefore frequently approximated as the difference, ΔT_{eq}, between

21   equilibrium near surface air temperatures obtained from two runs over a few decades with a slab ocean

22   model version which use the same calibration for the control and the experimental run. The first

23   column in Table 5 gives the ECS measured as ΔT_{eq} after a doubling of the atmospheric CO$_2$

24   concentrations (as described in Ch. 3). The number for CCSM4 is from Bitz et al. (2012). The 2

25   degree version was estimated with a smaller sensitivity (3.14 K) than the 1 degree version, while the 1

26   degree version NorESM1-Happi is less sensitive than the 2 degree version NorESM1-M.

27   Table 5 also lists estimates of the ECS based on linear regression between simultaneous values of

28   near-surface air temperature change ($\Delta T(t)$) and TOA radiation imbalance ($\Delta R(t)$) estimated at time t

29   after the abrupt quadrupling of atmospheric CO$_2$ (Gregory et al., 2004). Assuming negligible

30   contributions from time-varying feedbacks, the slope of the linear regression line between $\Delta R(t)$ and

31    $\Delta T(t)$ is the overall feedback parameter $\lambda_{reg} = -d\Delta R/d\Delta T$ (in units of W m^{-2} K^{-1}), while the

32   intercept at ΔT=0 approximates the instantaneous forcing $R_{f,reg}$, and the intercept ΔT_{reg} at $\Delta R = 0$

33   approximates the ECS. This estimate of R_f disregards rapid adjustment during the first year of the

34   simulation (Andrews et al., 2012). Table 5 lists all these quantities for the three models valid for CO$_2$

1   doubling. The independent estimate of the inferred TOA radiative forcing is R_{f0} = 3.5 W m^{-2} (Kay et

2   al., 2012), which is larger than the regression estimates for all three models, although the difference

3   for NorESM1-Happi is much smaller. The difference is normally ascribed to fast feedbacks during the

4   first year after the CO_2-increase, while the difference between ΔT_{reg} and ΔT_{eq} considered to reflect the

5   error of using linear regression due to slow feedbacks e.g. in the oceans (Senior and Mitchell, 2000).

6   Murphy (1995) proposed to use the remaining TOA radiative imbalance $\Delta R(t)$ at the time t to

7   approximate ECS. This approximation, termed the effective climate sensitivity, is:

8   $$\Delta T_{eff}(t) = \Delta T(t)R_f/(R_f - \Delta R(t)) \qquad (2)$$

9   Assuming the same linear relationship between $\Delta T(t)$ and $\Delta R(t)$, ΔT_{eff} should not depend on time,

10 but also in this case, slow feedback processes may do. In parallel to $\Delta T_{eff}(t)$ it is possible to define an

11 effective feedback parameter (Gettelman, 2012) $\lambda_{eff} = R_{f0}/\Delta T_{eff}$, which appears to be more

12 internally consistent than λ_{reg}, see Table 5, and we consider -1.22 W m^{-2} K^{-1} to be the more reliable

13 estimate of the feedback parameter for NorESM1. The values of ΔT_{eff} in Table 5 are averages of

14 annual values for the last 40 of the 150 simulation years of the abrupt 4xCO$_2$ experiments, and divided

15 by 2 for doubling rather than quadrupling. For the three models, ΔT_{reg} and ΔT_{eff} are almost equal and

16 the models are amongst the least sensitive of the CMIP5 models (e.g. Andrews et al., 2012).

17 The TCR can be estimated by similar simple methods as used for ECS, using the results from the

18 gradual 4xCO$_2$ experiment. The globally averaged change in near-surface air temperature at the time

19 of doubled atmospheric CO$_2$ (averaged over simulation years 60-80). An effective response that takes

20 into account the remaining TOA radiative imbalance can also be estimated by applying Eq. (2). The

21 values given in the rightmost columns in Table 5 present these estimates. While the approximate

22 values for ECS were close, the TRCs differ, with NorESM1-M having the smallest values. The

23 reasons for this can be related to the strong AMOC (Iversen et al., 2013) and features associated with

24 spatial resolution, but require further investigations beyond the scope of the present paper.

25 The experiments designed for estimating ECS and TCR are not meant to reflect realistic scenarios of

26 future developments. For this purpose, the RCPs were designed for CMIP5, and the fully coupled

27 NorESM1-Happi have extended Hist1 to year 2100 by assuming the changes defined in RCP 2.6, 4.5

28 and 8.5, were the numbers are pre-calculated values of the TOA radiative forcing at 2100 relative to

29 1850. In section 5 we address the targeting of temperature ceilings with simplified methods.

30 Fig. 5 includes the calculated projections of the fluxes at the top of the model atmosphere, the global

31 temperature at reference height, and the global precipitation rate. The results indicate that it takes time

32 until 2040-50 before considerable differences between the scenario projections are seen. This is also

33 the case for changes in the strength of the Atlantic Meridional Overturning Circulation (AMOC), see

Earth System
Dynamics
Discussions

1   Fig. 16. Notice that the AMOC in NorESM1-Happi towards 2100 for RCP8.5 is still stronger than

2   many other models for the present climate.

3   In Fig. 17 we see evidence of Arctic Amplification of the global signals of systematic temperature

4   change as well as variation. The apparent Arctic variability is likely to be exaggerated, since the

5   average is taken over less than 5% of the earth's surface (north of 65°N), and the average over any 5%

6   of the surface has larger variability than the global average. For the climate change signal, a rule of

7   thumb is that the Arctic temperature change is ca. twice that of the global.

8   The numbers in Table 6 are valid for the 30 years towards the end of the 21st century compared to the

9   end of the 20th (approximately). Unfortunately, we have not been able to run several ensemble

10   members, and we have no reliable estimate of signal-to-noise ratio. A simple "back-of-the-envelope"

11   calculation shows that RCP2.6 produces a 1.46 K global temperature increase towards 2100 relative to

12   1850, although this value does not represent a stable new equilibrium as assumed by the Paris

13   agreement. The average response for the CMIP5 archive is 1.55 K.

14   For simplicity, taking RCP2.6 with NorESM1-Happi to approximate the situation in a 1.5°C world, the

15   annual sea-ice area (both hemispheres) will be reduced by 8.2% (12.6%) compared to end 20th century,

16   the global precipitation amounts will be 2.2% (3.1%) larger, the continental precipitation will be 2.4%

17   (4.2%) larger, and the continental (P-E) will be 2.7% (6.8%) larger, all compared to end 20th century,

18   and completely based on the numbers from NorESM1-Happi. In comparison, the RCP4.5 projection

19   with NorESM1-Happi gives a 2.14 K warmer climate by the end of 21st century than in 1850 (2.40 K

20   for the CMIP5 archive). Using a similarly simple calculation assuming a factor 0.93 of the changes in

21   RCP4.5 to approximate a 2.0°C warmer world than in 1850, we arrive at the numbers given in the

22   brackets above. These numbers are based on single projections from one single model, and

23   accordingly must be used very carefully. Yet, they indicate that there can be considerable differences

24   between the climate of a 2.0°C world and a 1.5°C world. We continue to discuss this with more

25   robustness in the next section. If the RCP8.5 should turn out to be realized, we are facing a 3.7°C

26   world (according to the single NorESM1-Happi realization), with considerable larger impacts on sea-

27   ice and precipitation.

28

29   **5   Global Temperature Ceilings and Arctic Amplification**

30   **5.1   NorESM1-HappiAMIP and NorESM1-HappiSO**

31   With NorESM1-Happi, we have contributed to the experiments in the multi-model HAPPI project.

32   The target of the experiments is to investigate how important aspects of global warming may manifest

33   itself under two stabilisation scenarios of 1.5°C and 2.0°C warmer than the 1850 climate. The

Earth System Dynamics
Discussions
Open Access

1   challenge is to determine forcing conditions that will produce the temperature targets, and thus also

2   calculate other variables that characterize the climate state. Given that the climate system takes

3   centuries and longer to approach new equilibria after sustained changes in the TOA radiation balance,

4   it is not practically straightforward to apply coupled climate models for this purpose.

5   Simplified methods are required, but they should be based on the state of knowledge that present

6   climate and earth system models represent. Sanderson et al. (2017) proposed to emulate the results

7   from an advanced climate model with simplified methods. In HAPPI, Mitchell et al. (2017) proposed

8   to prescribe SST, sea-ice, and anthropogenic forcing elements and run models that couple atmosphere

9   and land but avoid the calculation of slow ocean processes and sea-ice. These are AMIP-type

10 experiments, and here we will identify our runs with for HAPPI as NorESM1-HappiAMIP.

11 The construction of driving input data to the AMIP experiments in HAPPI is thoroughly described by

12 Mitchell et al. (2017). They are observationally based (Taylor et al., 2012) for the present day climate

13 (PD, 2005-2016), but for the future temperature targets they are achieved by combining forcing data

14 for RCP2.6 and RCP4.5 for the year 2095, and associated data for SST from the model projections in

15 the CMIP5 archive. The future sea-ice is not directly taken from the CMIP5-models, partly because of

16 the huge variation in biases and partly because the models have common biases in the SH. In short, the

17 sea-ice in any point was fitted to the SSTs after establishing an observationally based linear relation

18 (by regression) between SST- and sea-ice anomalies for 1996-2015. The NorESM1-HappiAMIP data

19 cover 100 ensemble members of length 10 years (each after a 1-year spin-up) for PD, for the 1.5°C

20 world, and for the 2.0°C world, in all 3000 years of data. 25 additional ensemble members per period

21 have been run with high temporal resolution to enable dynamic downscaling of the results. The data

22 are available for download at http://portal.nersc.gov/c20c/data.html.

23 One shortcoming of pure AMIP-type runs where both SST and sea-ice are prescribed, is the missing

24 possibility to explicitly calculate the effects of feedback mechanisms associated with them. Arctic

25 amplification (AA) such as seen in evidence for in Fig. 17 is likely to be associated with such

26 feedbacks. Pithan and Mauritsen (2014) pointed out the lapse-rate and albedo feedbacks as important

27 causes of AA, and both are associated with low-level temperature changes in the Arctic. We have

28 therefore designed the slab-ocean model version NorESM1-HappiSO and calibrated the upper ocean

29 flux divergence of heat (Q_f) to emulate the NorESM1-HappiAMIP experiments as described in Ch. 3.

30 Three 310-year long experiments have been made for, respectively PD, 1.5°C, and 2.0°C. After a spin-

31 up of 45 years, a new equilibrium is considered reached in each case, leaving three equilibrated runs of

32 length 265 years. The results of these are compared to the NorESM1-HappiAMIP ensembles.

Earth System Dynamics
Discussions

5.2   Arctic Amplification and the 0.5^{o}C difference

In Table 7 we have defined a *Polar Amplification Factor" PAF* $= \Delta T_{Polar}/\Delta T_{Global}$, where the subscript Polar identifies an average over the area poleward of the 60° latitude circles for each hemisphere, and where T in this case is the 2 m temperature. The table shows results for PAF in both hemispheres together with the global change in 2 m temperature. Results for AMIP and SO are shown together with the single projections for the RCP2.6 and RCP4.5 scenarios. It is reassuring that both NorESM1-Happi AMIP and SO quite accurately hit the temperature targets, although the SO produces a slightly lower PD temperature. The fully coupled NorESM1-Happi confirms the negative temperature bias, and the increments are also somewhat larger. The PAF is considerably larger in the Arctic than in the Antarctic, and the AA is enhanced with the SO model compared to the AMIP. The latter includes the difference between the 2.0 and 1.5^{o}C worlds for which NH_PAF is 18% larger.

Table 8 shows similar statistics as Table 7, but for the NH extratropical winter and summer land temperatures, land precipitation rates, and sea-ice area. The SO model has a tendency to produce a colder winter climate than AMIP, which also manifests itself with a larger sea-ice area. In summer, however, these differences are much smaller. Probably the tendency towards colder climate, which is established as a systematic error for the fully coupled model, shows up during winter with the SO model. Furthermore, the 1.5^{o}C-PD response is a smaller reduction in sea-ice area with SO than in the prescribed data for AMIP for both seasons. For the 2.0^{o}C-PD response this is only seen during winter, while the sea-ice area is more reduced in summer. These features are also reflected in the temperatures and precipitation over land.

The increases in 2 m temperatures and the precipitation over NH land is larger for SO than for AMIP in summer (JJA), but not in winter (DJF). For the difference 2.0^{o}C -1.5^{o}C, the SO response is larger than AMIP for summer precipitation and summer sea-ice area. Otherwise, the differences are negligible, and even of opposite sign for the winter sea-ice area.

The sea-ice area for the PD AMIP-runs in DJF (Table 8) is considerably smaller than the observed for March in Table 4, although also the first is based on observations. The sea-ice area is at its maximum in March, and a difference is to be expected. The difference is considerably smaller for the SO and fully coupled model (less than 50%). Table 4 shows that NorESM1-Happi has a negative bias in March, while Table 8 indicates a positive bias averaged for the three winter months (DJF). Assuming that the observations in the two tables are internally consistent (which is a relevant comment since the time periods for observations are not the same) it appears that Arctic sea-ice cover grows too fast during the early winter months and too slow towards the March maximum. More in-depth studies are required to establish if the early winter over-estimate is due to a cold-bias tendency of NorESM1-HappiSO (as well as in NorESM1-Happi) that is

Earth System
Dynamics
Discussions

1   amplified by the prognostic sea-ice cover in the SO model, or if it reflects a natural process of reduced

2   feedbacks associated with sea-ice and SST during winter darkness which is not well represented in the

3   model.

4   **5.3   Cyclone activity and blocking**

5   As for the fully coupled NorESM1-Happi, we have calculated the extratropical cyclone activity and

6   blocking occurrence. Fig. 18 shows the seasonal cyclone activity in the PD AMIP runs compared to

7   ERA-Interim and the difference in cyclone activity between the SO and AMIP for PD. When

8   comparing with the corresponding Fig. 13 for the fully coupled NorESM1 models, it should be noted

9   that the colour scale is finer in Fig 18 by approximately a factor 2 for the plots on the left, and a factor

10   3 for the plots on the right. The absolute values of the biases are smaller for both the AMIP and SO,

11   and while it was clear that all biases were negative for the coupled models, i.e. generally too low

12   cyclone activity, the AMIP and SO results have biases of both signs. A systematic displacement of the

13   cyclone activity closer to the Arctic than in ERA-Interim is a general impression. In the Atlantic-

14   European sector, there is too much cyclone activity over the continent in winter and spring, and too

15   little activity in the branch over the Nordic Seas between Scandinavia and Greenland. These biases are

16   not reduced in the SO runs. Instead they rather seem to be slightly larger, with a few exceptions. In the

17   autumn the positive biases in AMIP results over the Arctic are reduced in the SO runs.

18   Fig. 19 shows the changes in cyclone activity from PD to a 1.5°C world. For reference, results are also

19   shown for the RCP2.6 of the fully coupled NorESM1-Happi, since RCP2.6 produces approximately

20   1.5°C higher 2 m global temperatures than the piControl (see Table 6). Except for the summer months

21   when the response is small, the SO response is considerably larger than the AMIP response, and this is

22   particularly evident for winter and spring. The signal is dominated by reduced extratropical cyclone

23   activity, which is also seen in the RCP2.6 scenario of NorESM1-Happi. Except for the autumn

24   months, the AMIP response appears artificially small, although we do not know how the real response

25   will be. To the extent that reduced activity can be interpreted as slower propagation of cyclone waves

26   in the westerlies, this can be associated with reduced low-level meridional temperature gradients

27   associated with the high-latitude warming over the Arctic (e.g. Francis and Vavrus, 2012; Screen and

28   Simmonds, 2013). In winter the SO-response include an apparent northward displacement of the

29   cyclone activity in the Atlantic sector of the Arctic. We have also looked at the difference in cyclone

30   activity between a 1.5°C and a 2.0°C world for SO and AMIP. The differences are small in all seasons

31   although there are patches of statistically significant differences (not shown).

32   Fig. 20 shows seasonal statistics for blocking occurrence (the vTM index) for the AMIP runs at PD,

33   compared to ERA-Interim results. The results for the SO runs are almost identical. The results are

34   slightly better than for the coupled NorESM1 models (Fig. 14), but there still are problems in

1   representing sufficient blocking occurrence in the Atlantic sector. Fig. 21 shows the changed

2   occurrence of blocking for the 1.5^{o}C -PD difference and for the 2.0^{o}C -1.5^{o}C difference. Both AMIP

3   results and SO results are shown. Statistically significant changes (at the 5 % level) are more frequent

4   with the SO runs than the AMIP, and the signals of changed blocking occurrence are also considerably

5   stronger in the SO results (hence the different units on the y-axes). However, there are several cases

6   for which the AMIP runs show increased (decreased) blocking occurrence with statistical significance,

7   which are not confirmed by increased (decreased) blocking occurrence in the results from the SO

8   model. For example, in winter for the 1.5^{o}C -PD difference, the AMIP-results predict a statistically

9   significant reduction in blocking occurrence at 240°E, while the SO-results predict a strong and

10   statistically significant increase in blocking occurrence. The level of significance is 5%, so there still is

11   a possibility that this is by chance, but it can be a consequence of the feedbacks with SST and sea-ice

12   allowed in the SO-model.

13   Considering the difference between a 1.5 and a 2.0^{o}C world, the SO results predict reduced occurrence

14   of blocking in Europe in winter and autumn and increased occurrence in central Eurasia and the

15   Pacific Ocean. The strongest signal is seen in Atlantic-European sector in spring, where a statistically

16   significant increase from PD to the 1.5^{o}C world is strengthened by a further statistically significant

17   increase from 1.5 to 2.0^{o}C. There are several cases with considerable changes of blocking occurrence

18   between a 1.5 and a 2.0^{o}C world, e.g., a reduced occurrence in autumn between 20 and 60°E, and an

19   increased occurrence around 90°E in summer.

20   **5.4   Arctic sea-ice reduction**

21   The extension, thickness and concentration of sea-ice are important variables in the climate system.

22   Fig. 22 show the extension and concentration of Arctic sea-ice in March and September calculated

23   with NorESM1-HappiSO. For PD the concentration map from the model is compared to observational

24   data from OSI-SAF (2017). The quality of the model-data is better in March than in September, when

25   the model seems to underestimate the ice-concentration. For the temperature targets, the sea-ice in

26   March is predominantly reduced along the edges. However, it should be borne in mind that the SO

27   model may be too cold (Table 8). In September, the reduction in sea-ice concentration (and extension)

28   is moderate for the 1.5-PD change, but the further reduction from 1.5 to 2.0^{o}C is substantial.

29   The latter is indeed confirmed by Fig. 23 which shows a histogram of SO-model calculated relative

30   occurrence of NH September sea-ice in different classes of extent for PD and the two temperature

31   targets. For PD the model tends to produce too few cases with largest extent. Looking at the possibility

32   of having ice-free Arctic September minima, i.e. the fraction of cases in the class between 0 and 1x10^6

33   km^2, the model predict probability of this occurrence to be practically zero under PD conditions, a tiny

34   fraction in the 1.5^{o}C world, and ca. 40 % for the 2.0^{o}C world. The difference between the two

1   temperature targets is therefore potentially very large for the Arctic sea-ice in summer-fall, a result

2   that was also found by Sanderson et al. (2017).

3

4   **6   Summary and Conclusions**

5   This paper presents a validation of model tools which are used to study the significance of differences

6   in the global climate between a world with a stable 2 m temperature which is 1.5°C higher and 2.0°C

7   higher than in 1850. The incitement is the outcome of the Paris protocol that a Special Report from

8   IPCC is under development. The state-of-science model tools we have used for this purpose is

9   basically a slightly upgraded versions of the atmosphere and land models in the coupled NorESM1-M,

10   which was used for CMIP5 (Bentsen et al., 2013; Iversen et al., 2013, Kirkevåg et al., 2013).

11   A proper validation of such tools requires a documentation of its performance fully coupled to a deep

12   ocean model and a sea-ice model. The first part of results for this paper (Ch. 4) presents a selection of

13   results from a quite complete set of the fully coupled model runs with NorESM1-Happi. The name

14   Happi comes from our association with the multi-model HAPPI project (Mitchell et al., 2016 and

15   2017), for which large ensembles of AMIP-type experiments are made and analysed. The second part

16   of results (Ch. 5) focuses results from the HAPPI AMIP runs with the atmosphere and land modules of

17   NorESM1-Happi, complemented with results from a specially designed slab-ocean (SO) version of the

18   model (NorESM1-HappiSO) which includes a fully dynamic-thermodynamic sea-ice module. Our

19   main reason for complementing with a SO model, is that the AMIP-runs pre-define aspects of the

20   Arctic Amplification (AA) which do not allow adjustments by on-line feedbacks. The SO-model

21   allows changes in SST and sea-ice which can influence both surface albedo and the atmospheric

22   temperature lapse rate, which both are major elements in producing AA (Pithan and Mauritsen, 2014).

23   The results and discussions in Ch. 4 show that NorESM1-Happi is a valid model tool for climate

24   research at the present state of science. The stability of long-term climate properties over the 500-year

25   pre-industrial run is at least as good as for NorESM1-M, except for the AMOC which is strong and

26   has a positive trend. The model has double resolution and a few improvements in physical

27   parameterizations compared to the original CMIP5 version. This partly increases some of the biases,

28   cloud cover, 2 m temperature, and the strength of the AMOC in particular, but considerably improves

29   the Arctic sea-ice thickness and reduces the biases in extratropical cyclone activity and occurrence of

30   blocking in the northern hemisphere. Although the intensity of the water cycle is exaggerated (by

31   6.7% globally), the atmospheric residence time of water vapour and the budget of transport between

32   oceans and continents are reasonable. The model represents the Madden-Julian Oscillation with

33   reduced errors than in NorESM1-M, and the return period of ENSO events is slightly reduced, but

34   with too low amplitudes. The model's standard estimates of climate sensitivity are still in the lower

Earth System
Dynamics
Discussions

1   range amongst global climate models. With reference to the question of differences between a 1.5^{o}C

2   and a 2.0^{o}C world, NorESM1-Happi shows a considerable difference in response between the RCP2.6

3   and the RCP4.5 scenarios.

4   In Ch. 5 we saw that the NH extratropical cyclone activity is not improved in the SO model results

5   compared to the AMIP results, and for occurrence of NH blocking the differences are negligible. The

6   SO results also show stronger responses than the AMIP results to a global change. In particular, the

7   SO result reduces the NH extratropical cyclone activity considerably. Changes in the occurrence of

8   blocking are larger, although the total signals of change in response in a warmer world are mixed. The

9   SO-model simulates considerable differences in the reduction of sea-ice in the Arctic between a 1.5^{o}C

10 and a 2.0^{o}C world. Ice-free summer conditions in the Arctic is estimated to be very rare for the 1.5^{o}C

11 case, but to occur 40% of the time for the 2.0^{o}C case. These results agree with some fully coupled

12 models, but need to be further confirmed.

13

14 **7   Code and Data Availability**

15 The source code for NorESM1-Happi is not open for anyone to download, since parts of the code is

16 imported from several code development centres. The code can be made available within the

17 framework of an agreement. Data from the model experiments made with the model can be made

18 available as well, e.g. NCC / NorESM1-HAPPI from http://portal.nersc.gov/c20c/data.html. Contacts:

19 oyvindse@met.no and ingo.bethke@uni.no.

20

31

Earth System
Dynamics
Discussions

EGU

1   **References**

2   Abdul-Razzak, H. and Ghan, S. J.: A parameterization of aerosol activation, Part 2: Multiple aerosol
3   types, J. Geophys. Res., 105, 6837–6844, 2000.

4   Acosta Navarro, J.C., V. Varma, I. Riipinen, Ø. Seland, A. Kirkevåg, H. Struthers, T. Iversen, H.-C.
5   Hansson, and A. M. L. Ekman: Amplification of Arctic warming by past air pollution reductions in
6   Europe. Nature Geoscience, 03, DOI:10.1038/ngeo2673, 2016.

7   Adler, R. F., G. J. Huffman, A. Chang, R. Ferraro, P. Xie, J. Janowiak, B. Rudolf, U. Schneider, S.
8   Curtis, D. Bolvin, A. Gruber, J. Susskind, and P. Arkin: The Version 2 Global Precipitation
9   Climatology Project (GPCP) Monthly Precipitation Analysis (1979-Present). J. Hydrometeor., 4,1147-
10   1167. 2003.

11   Allen, R. J., and W. Landuyt: The vertical distribution of black carbon in CMIP5 models: Comparison
12   to observations and the importance of convective transport, J. Geophys. Res. Atmos., 119, 4808–4835,
13   doi:10.1002/2014JD021595, 2014.

14   Ammann, C. M., G. A. Meehl, W. M. Washington, and C. Zender: A monthly and latitudinally
15   varying volcanic forcing dataset in simulations of 20th century climate. Geophys. Res. Lett., 30, 1657,
16   doi:10.1029/2003GL016875. 2003

17   Anderson, K. and Nevins, J.: Planting Seeds So Something Bigger Might Emerge: The Paris
18   Agreement and the Fight Against Climate Change, Socialism and Democracy, 30, 209–218, 2016.

19   Andrews, T., J. M. Gregory, M. J. Webb, and K. E. Taylor: Forcing, feedbacks and climate sensitivity
20   in CMIP5 coupled atmosphere-ocean climate models. Geophys. Res. Lett., 39, L09712,
21   Doi:10.1029/2012gl051607, 2012

22   Antonov, J. I., Seidov, D., Boyer, T. P., Locarnini, R. A., Mishonov, A. V., Garcia, H. E., Baranova,
23   O. K., Zweng, M. M., and Johnson, D. R.: World Ocean Atlas 2009, Volume 2: Salinity, in: NOAA
24   Atlas NESDIS 69, edited by: Levitus, S., U.S. Government Printing Office, Washington, DC, 184 pp.,
25   2010.

26   Assmann, K. M., Bentsen, M., Segschneider, J., and Heinze, C.: An isopycnic ocean carbon cycle
27   model, Geosci. Model Dev., 3, 143–167, doi:10.5194/gmd-3-143-2010, 2010.

28   Arrhenius, S.: On the influence of carbonic acid in the air upon the temperature of the ground, Philos.
29   Mag. J. Sci. 5, 237-276.

30   Barnes. E. A. and Polvani, L. M.: CMIP5 Projections of Arctic Amplification, of the North
31   American/North Atlantic Circulation, and of Their Relationship. J. Climate, 28, 5254-5270. doi:
32   10.1175/JCLI-D-14-00589.1, 2015.

1   Bentsen, M., I. Bethke, J. B. Debernard, T. Iversen, A. Kirkevåg, Ø. Seland, H. Drange, C. Roelandt,

2   I. A. Seierstad, C. Hoose, J. E. Kristjánsson**:** The Norwegian Earth System Model, NorESM1-M—Part

3   1: Description and basic evaluation of the physical climate. Geosci. Model Dev., 6, 687–720,

4   doi:10.5194/gmd-6-687-2013

5   Bitz, C. M., K. M. Shell, P. R. Gent, D. A. Bailey, G. Danabasoglu, K. C. Armour, M. M. Holland, J.

6   T. Kiehl: Climate Sensitivity of the Community Climate System Model, Version 4. J. Climate, 25,

7   3053–3070. doi: http://dx.doi.org/10.1175/JCLI-D-11-00290.1. 2012.

8   Blackmon, M. L.: A climatological spectral study of the 500 mb geopotential height of the Northern

9   Hemisphere. J. Atmos. Sci., 33, 1607–1623. 1976

10   Boer, G. J. andYu, B.: Climate sensitivity and response. Clim. Dyn. 20, 415–429. DOI

11   10.1007/s00382-002-0283-3. 2003.

12   Boucher, O., Bellassen, V., Benveniste, H., Ciais, P., Criqui, P., Guivarch, C., Le Treut, H., Mathy, S.,

13   and Séférian, R.: Opinion: In the wake of Paris Agreement, scientists must embrace new directions for

14   climate change research, P. Natl. Acad. Sci. USA, 113, 7287–7290, 2016.

15   Bratseth, A. M.: Eddy Acceleration of the Mean Flow in the Atmosphere. J. Atmos. Sci., 58, 3328–

16   3339. 2001.

17   Bratseth, A. M.: Zonal-mean transport characteristics of ECMWF re-analysis data. Q. J. R. Meteorol.

18   Soc., 129, 2331–2346. doi: 10.1256/qj.02.90. 2003.

19   Briegleb, B. P. and Light, B.: A Delta-Eddington Mutiple Scattering Parameterization for Solar

20   Radiation in the Sea Ice Component of the Community Climate System Model, Tech. Rep.

21   NCAR/TN-472+STR, National Center for Atmospheric Research, Boulder, Colorado, USA, 2007.

22   Cassou, C.: Intraseasonal interaction between the Madden–Julian oscillation and the North Atlantic

23   oscillation, Nature, 455, 523–527, doi:10.1038/nature07286, 2008.

24   Cohen, J., J. A. Screen, J. C. Furtado, M. Barlow, D. Whittleston, D. Coumou, J. Francis, K. Dethloff,

25   D. Entekhabi, J. Overland, and J. Jones: Recent Arctic amplification and extreme mid-latitude

26   weather, Nature Geoscience 7, 627–637, 2014.

27   Collins, W. D., Rasch, P. J., Boville, B. A., Hack, J. J., McCaa, J. R., Williamson, D. L., and Briegleb,

28   B. P.: The formulation and atmospheric simulation of the community atmosphere model version, J.

29   Climate, 19, 2144–2161, 2006.

30   Dee, D. P., Uppala, S. M., Simmons, A. J., Berrisford, P., Poli, P., Kobayashi, S., Andrae, U.,

31   Balmaseda, M. A., Balsamo, G., Bauer, P., Bechtold, P., Beljaars, A. C. M., van de Berg, L., Bidlot, J.,

32   Bormann, N., Delsol, C., Dragani, R., Fuentes, M., Geer, A. J., Haimberger, L., Healy, S. B.,

33   Hersbach, H., Hólm, E. V., Isaksen, L., Kållberg, P., Köhler, M., Matricardi, M., McNally, A. P.,

Earth System
Dynamics
Discussions

1 Monge-Sanz, B. M., Morcrette, J.-J., Park, B.-K., Peubey, C., de Rosnay, P., Tavolato, C., Thépaut, J.-
2 N. and Vitart, F., The ERA-Interim reanalysis: configuration and performance of the data assimilation
3 system. Q.J.R. Meteorol. Soc., 137: 553–597. doi: 10.1002/qj.828, 2011.

4 Donlon, C. J., M. Martin, J. D. Stark, J. Roberts-Jones, E. Fiedler and W. Wimmer: The Operational
5 Sea Surface Temperature and Sea Ice analysis (OSTIA). *Remote Sensing of the Environment.* doi:
6 10.1016/j.rse.2010.10.017, 2011.

7 Eyring, V., S. Bony, G. A. Meehl, C. A. Senior, B. Stevens5, R. J. Stouffer6, and K. E. Taylor:
8 Overview of the Coupled Model Intercomparison Project Phase 6 (CMIP6) experimental design and
9 organization. Geosci. Model Dev., 9, 1937–1958, doi:10.5194/gmd-9-1937-2016, 2016.

10 Feldl, N., B. Anderson, and S. Bordoni: Atmospheric eddies mediate lapse rate feedback and Arctic
11 amplification. J. Climate. doi:10.1175/JCLI-D-16-0706.1, in press, 2017.

12 Francis, J. A., and S. J. Vavrus: Evidence linking Arctic amplification to extreme weather in mid-
13 latitudes. Geophysical Research Letters, 39 (6), doi:10.1029/2012GL051000, 2012.

14 Gent, P.R., G. Danabasoglu, L. J. Donner, M. M. Holland, E. C. Hunke, S. R. Jayne, D. M. Lawrence,
15 R. B. Neale, P. J. Rasch, M. Vertenstein, P. H. Worley, Z.-L. Yang, and M. Zhang: The Community
16 Climate   System   Model   Version   4.   J.   Climate,   24,   4973–4991.   doi:
17 http://dx.doi.org/10.1175/2011JCLI4083.1 2011.

18 Gettelman, A., J. E. Kay, K. M. Shell: The Evolution of Climate Sensitivity and Climate Feedbacks in
19 the Community Atmosphere Model. J. Climate, 25, 1453–1469. doi: http://dx.doi.org/10.1175/JCLI-
20 D-11-00197.1. 2012.

21 Giorgi, F., Im, E.-S., Coppola, E., Diffenbaugh, N. S., Gao, X . J., Mariotti, L., and Shi, Y.: Higher
22 Hydroclimatic   Intensity   with   Global   Warming.   J.   Climate,   24,   5309-5324,   doi:
23 10.1175/2011JCLI3979.1, 2011.

24 Greenwald, T. J.: A 2 year comparison of AMSR-E and MODIS cloud liquid water path observations,
25 Geophys. Res. Lett., 36, L20805, doi:10.1029/2009GL040394, 2009.

26 Hansen, J., R. Ruedy, M. Sato, and K. Lo: Global surface temperature change. *Rev. Geophys.*, 48,
27 RG4004, doi:10.1029/2010RG000345, 2010.

28 Harrison, E. F., Minnis, P., Barkstrom, B. R., Ramanathan, V., Cess, R. D., and Gibson, G. G.:
29 Seasonal variation of cloud radiative forcing derived from the earth radiation budget experiment, J.
30 Geophys. Res., 95, 18687–18703, 1990.

31 Hendon, H. H., Wheeler, M. C., and Zhang, C.: Seasonal Dependence of the MJO–ENSO
32 Relationship, J. Climate, 20, 531–543, doi:10.1175/JCLI4003.1, 2007.

Earth System
Dynamics
Discussions

1   Holland, M. M., and C. M. Bitz: Polar amplification of climate change in coupled models, Clim. Dyn.,
2   21, 221–232, 2003.

3   Holland, M. M., Bailey, D. A., Briegleb, B. P., Light, B., and Hunke, E.: Improved sea ice shortwave
4   radiation physics in CCSM4: the impact of melt ponds and aerosols on arctic sea ice, J. Climate, 25,
5   1413–1430, doi:10.1175/JCLI-D-11-00078.1, 2012.

6   Huffman, G. J., Adler, R. F., Bolvin, D. T., and Gu, G.: Improving the global precipitation record:
7   GPCP Version 2.1, Geophys. Res. Lett., 36, L17808, doi:10.1029/2009GL040000, 2009.

8   Hulme, M.: 1.5 _C and climate research after the Paris Agreement, Nat. Clim. Change, 6, 222–224,
9   2016.

10   Hurrell, J. W., J. J. Hack, D. Shea, J. M. Caron, and J. Rosinski.: A New Sea Surface Temperature and
11   Sea Ice Boundary Dataset for the Community Atmosphere Model. J. Climate, 21, 5145-5153,
12   doi.org/10.1175/2008JCLI2292.1, 2008.

13   IPCC, 2013: Climate Change 2013: The Physical Science Basis. Contribution of Working Group I to
14   the Fifth Assessment Report of the Intergovernmental Panel on Climate Change [Stocker, T.F., D.
15   Qin, G.-K. Plattner, M. Tignor, S.K. Allen, J. Boschung, A. Nauels, Y. Xia, V. Bex and P.M. Midgley
16   (eds.)]. Cambridge University Press, Cambridge, United Kingdom and New York, NY, USA, 1535pp,
17   2013.

18   Iversen, T., Bentsen, M., Bethke, I., Debernard, J. B., Kirkevåg, A., Seland, Ø., Drange, H.,
19   Kristjansson, J. E., Medhaug, I., Sand, M., and Seierstad, I. A.: The Norwegian Earth System Model,
20   NorESM1-M – Part 2: Climate response and scenario projections, Geosci. Model Dev., 6, 389–415,
21   doi:10.5194/gmd-6-389-2013, 2013.

22   James, R., Washington, R., Schleussner, C.-F., Rogelj, J., and Conway, D.: Characterizing half-a-
23   degree difference: a review of methods for identifying regional climate responses to global warming
24   targets, WIREs Clim Change, 8:e457. doi: 10.1002/wcc.457doi:10.1002/wcc.457, 2017.

25   Jiang, J.H., Su, H, Zhai, C., Perun, V.S and co-authors: Evaluation of Cloud and Water Vapor
26   Simulations in CMIP5 Climate Models Using NASA "A-Train" Satellite Observations" J. Geophys.
27   Res., 117, D14105, 24 PP., doi:10.1029/2011JD017237, 2012.

28   Jung, T., M.J. Miller, T.N. Palmer, P. Towers, N. Wedi, D. Achuthavarier, J. M. Adams, E. L.
29   Altshuler, B. A. Cash, J. L. Kinter III, L. Marx, and C. Stan, and K. I. Hodges: High-Resolution
30   Global Climate Simulations with the ECMWF Model in Project Athena: Experimental Design, Model
31   Climate, and Seasonal Forecast Skill. *J. Climate*, **25**, 3155–3172. doi: http://dx.doi.org/10.1175/JCLI-
32   D-11-00265.1. 2012.

Earth System
Dynamics
Discussions

1 Jung, M., Reichstein, M., Margolis, H. A., Cescatti, A., Richardson, A. D., Arain, M. A., Arneth, A.,

2 Bernhofer, C., Bonal, D., Chen, J., Gianelle, D., Gobron, N., Kiely, G., Kutsch, W., Lasslop, G., Law,

3 B. E., Lindroth, A., Merbold, L., Montagnani, L., Moors, E. J., Papale, D., Sottocornola, M., Vaccari,

4 F., and Williams, C.: Global patterns of land-atmosphere fluxes of carbon dioxide, latent heat, and

5 sensible heat derived from eddy covariance, satellite, and meteorological observations, J. Geophys.

6 Res., 116, G00J07, doi:10.1029/2010JG001566, 2011.

7 Kanamitsu, M., Ebisuzaki, W., Woollen, J., Yang, S. K., Hnilo, J. J., Fiorino, M., and Potter, G. L.:

8 NCEP-DOE AMIP–II reanalysis (R-2), Bull. Amer. Meteor. Soc., 83, 1631–1643,

9 doi:10.1175/BAMS-83-11-1631, 2002.

10 Kay, J.E., Holland, M.M., Bitz, C.M., Blanchard-Wrigglesworth, E., Gettelman, A., Conley, A., and

11 Bailey, D.: The influence of local feedbacks and northward heat transport on the equilibrium Arctic

12 climate response to increased greenhouse gas forcing. J. Climate, early online release. doi:

13 http://dx.doi.org/10.1175/JCLI-D-11-00622.1 2012.

14 Kiehl, J. T. and Trenberth, K. E.: Earth's annual global mean energy budget, Bull. Amer. Meteor.

15 Soc., 78, 197–208, 1997.

16 Kim, S. T. and Yu, J-Y.: The Two Types of ENSO in CMIP5 Models. Geophys. Res. Lett., 39,

17 L11704, doi:10.1029/2012GL052006, 2012.

18 Kirkevåg, A., Iversen, T., Seland, Ø., Hoose, C., Kristjánsson, J. E., Struthers, H., Ekman, A. M. L.,

19 Ghan, S., Griesfeller, J., Nilsson, E. D., and Schulz, M.: Aerosol–climate interactions in the

20 Norwegian Earth System Model – NorESM1-M, Geosci. Model Dev., 6, 207–244, doi:10.5194/gmd-

21 6-207-2013, 2013.

22 Knutson, T.: FMS slab ocean model technical documentation, 2003. [Visited online 2017 at

23 http://www.gfdl.noaa.gov/fms-slab-ocean-model-technical-documentation.]

24 Lamarque, J. F., Bond, T. C., Eyring, V., Granier, C., Heil, A., Klimont, Z., Lee, D., Liousse, C.,

25 Mieville, A., Owen, B., Schultz, M. G., Shindell, D., Smith, S. J., Stehfest, E., Van Aardenne, J.,

26 Cooper, O. R., Kainuma, M., Mahowald, N., McConnell, J. R., Naik, V., Riahi, K., and van Vuuren,

27 D. P.: Historical (1850–2000) gridded anthropogenic and biomass burning emissions of reactive gases

28 and aerosols: Methodology and application. Atmos. Chem. Phys. Discuss., 10, C922–C926. 2010.

29 Large, W. G. and Yeager, S.: Diurnal to decadal global forcing for ocean and sea-ice models: the data

30 sets and flux climatologies, Tech. Rep. NCAR/TN-460+STR, National Center for Atmospheric

31 Research, Boulder, Colorado, USA, 2004.

32 Large, W. G. and Yeager, S. G.: The global climatology of an interannually varying air-sea flux data

33 set, Clim. Dynam., 33, 341–364, doi:10.1007/s00382-008-0441-3, 2008.

Earth System
Dynamics
Discussions

1 Lean, J., G. Rottman, J. Harder, and G. Kopp: SORCE contributions to new understanding of global

2 change and solar variability. Sol. Phys., 230, 27–53. 2005.

3 L'Ecuyer, T. S., Wood, N. B., Haladay, T., Stephens, G. L., and Stackhouse Jr., P. W.: Impact of

4 clouds on atmospheric heating based on the R04 CloudSat fluxes and heating rates data set, J.

5 Geophys. Res., 113, D00A15, doi:10.1029/2008JD009951, 2008.

6 Legates, D. R. and Willmott, C. J.: Mean seasonal and spatial variability in gauge-corrected, global

7 precipitation, Int. J. Climatol., 10, 111–127, 1990.

8 Locarnini, R. A., Mishonov, A. V., Antonov, J. I., Boyer, T. P., Garcia,H. E., Baranova, O. K., Zweng,

9 M. M., and Johnson, D. R.: World Ocean Atlas 2009, Volume 1: Temperature, in: NOAA Atlas

10 NESDIS 68, edited by: Levitus, S., US Government Printing Office, Washington, D.C., 184 pp., 2010.

11 Loeb, N. G., Kato, S., Loukachine, K., and Manalo-Smith, N.: Angular distribution models for top-of-

12 atmosphere radiative flux estimation from the clouds and the earths radiant energy system instrument

13 on the Terra satellite, Part I: Methodology, J. Atmos. Ocean. Tech., 22, 338–351,

14 doi:10.1175/JTECH1712.1, 2005.

15 Loeb, N. G., Wielicki, B. A., Doelling, D. R., Smith, G. L., Keyes, D. F., Kato, S., Manalo-Smith, N.,

16 andWong, T.: Toward optimal closure of the earth's top-of-atmosphere radiation budget, J. Climate,

17 22, 748–766, doi:10.1175/2008JCLI2637.1, 2009.

18 Loeb, N. G., Lyman, J. M., Johnson, G. C., Allan, R. P., Doelling, D. R., Wong, T., Soden, B. J., and

19 Stephens, G. L.: Observed changes in top-of-the-atmosphere radiation and upper-ocean heating

20 consistent within uncertainty, Nat. Geosci., 5, 110–113, doi:10.1038/ngeo1375, 2012.

21 Madden, R. A. and Julian, P. R.: Detection of a 40–50 day oscillation in the zonal wind in the Tropical

22 Pacific, J. Atmos. Sci., 28, 702–708, 1971.

23 Manabe S, Stouffer RJ (1980) Sensitivity of a global climate model to an increase of CO_2

24 concentration in the atmosphere. J Geophys Res 85: 5529–5554

25 Mitchell, D., James, R., Forster, P., Betts, R., Shiogama, H., and Allen, M.: Realizing the impacts of a

26 1.5 _C warmer world., Nat. Clim. Change, 6, 735–737, doi:10.1038/nclimate3055, 2016.

27 Mitchell, D., AchutaRao, K., Allen, M., Bethke, I., Forster, P., Fuglestvedt, J., Gillett, N., Haustein,

28 K., Iverson, T., Massey, N., Schleussner, C.-F., Scinocca, J., Seland, Ø., Shiogama, H., Shuckburgh,

29 E., Sparrow, S., Stone, D., Wallom, D., Wehner, M., and Zaaboul, R.: Half a degree Additional

30 warming, Projections, Prognosis and Impacts (HAPPI): Background and Experimental Design,

31 Geosci. Model Dev., 10, 571–583. doi:10.5194/gmd-10-571-2017, 2017.

Earth System
Dynamics
Discussions

1   Mitchell, T. D. and Jones, P. D.: An improved method of constructing a database of monthly climate

2   observations and associated high-resolution grids, Int. J. Climatol., 25, 693–712,

3   doi:10.1002/joc.1181, 2005.

4   Morice, C. P., Kennedy, J. J., Rayner, N. A., and Jones, P. D.: Quantifying uncertainties in global and

5   regional temperature change using an ensemble of observational estimates: the HadCRUT4 data set, J.

6   Geophys. Res., 117, D08101, doi:10.1029/2011JD017187, 2012.

7   Murphy, D. M.: Transient response of the Hadley Centre coupled ocean-atmosphere model   to

8   increasing carbon dioxide: Part III. Analysis of global-mean response using simple models. J. Climate,

9   8, 495–514. doi: http://dx.doi.org/10.1175/1520-0442(1995)008<0496:TROTHC>2.0.CO;2. 1995.

10 Neale, R. B., J. H. Richter, and M. Jochum: The impact of convection on ENSO: From a delayed

11 oscillator to a series of events. J. Climate, 21, 5904–5924. 2008.

12 Neale, R. B, J. H. Richter, A. J. Conley, S. Park, P. H. Lauritzen, A. Gettelman, D. L. Williamson, P.

13 J. Rasch, S. J. Vavrus, M. A. Taylor. W. D. Collins, M. Zhang, S-J. Lin: Description of the NCAR

14 Community Atmosphere Model (CAM 4.0), NCAR TECHNICAL NOTE, April 2010.

15 Neale, R. B., J. H. Richter, S. Park, P. H. Lauritzen, S. J. Vavrus, P. J. Rasch, M. Zhang: The mean

16 climate of the Community Atmosphere Model (CAM4) in forced SST and fully coupled experiments.

17 J. Climate 26, 5150-5168. doi: 10.1175/JCLI-D-12-00236.1, 2013.

18 O'Dell, C. W., Wentz, F. J., and Bennartz, R.: Cloud liquid water path from satellite-based passive

19 microwave observations: a new climatology over the global oceans, J. Climate, 21, 1721–1739,

20 doi:10.1175/2007JCLI1958.1, 2008.

21 Onogi, K., Tsutsui, J., Koide, H., Sakamoto,M., Kobayashi, S., Hatsushika, H., Matsumoto, T.,

22 Yamazaki, N., Kamahori, H., Takahashi, K., Kadokura, S., Wada, K., Kato, K., Oyama, R., Ose, T.,

23 Mannoji, N., and Taira, R.: The JRA-25 reanalysis, J. Meteor. Soc. Jpn., 85, 369–432, 2007.

24 OSI-SAF, 2017: EUMETSAT Ocean and Sea Ice Satellite Application Facility. Global sea ice

25 concentration climate data record 1979-2015 (v2.0, 2017), [Online]. Norwegian and Danish

26 Meteorological Institutes. doi: 10.15770/EUM_SAF_OSI_0008

27 Otterå, O. H., M. Bentsen, H. Drange, and L. Suo: External focing as a metronome for Atlantic

28 multidecadal variability, Nature Geosci., doi: 10.1038/NGEO955. 2010.

29 Pelly, J. L. and B. J. Hoskins: A new perspective on blocking. J. Atmos. Sci., 60,743–755. 2003.

30 Peters, G. P.: The "best available science" to inform 1.5 _C policy choices, Nat. Clim. Change, 6,

31 646–649, doi:10.1038/nclimate3000, 2016.

Earth System
Dynamics

Discussions

1   Pithan, F. and T. Mauritsen: Arctic amplification dominated by temperature feedbacks in
2   contemporary climate models. Nature Geoscience, **7**, 181-184. doi:10.1038/ngeo2071, 2014.

3   Rasch, P. J., D. B. Coleman, N. Mahowald, D. L. Williamson, S.-J. Lin, B. A. Boville, and P. Hess:
4   Characteristics of atmospheric transport using three numerical formulations for atmospheric dynamics
5   in a single GCM framework. J. Climate, 19**,** 2243–2266. 2006.

6   Rayner, N. A., D. E. Parker, E. B. Horton, C. K. Folland, L. V. Alexander, D. P. Rowell, E. C. Kent,
7   and A. Kaplan: Global analyses of sea surface temperature, sea ice, and night marine air temperature
8   since the late nineteenth century. J. Geophys. Res., 108 (D14), doi:10.1029/2002JD002670. 2003.

9   Richter, J. H., and P. J. Rasch: Effects of convective momentum transport on the atmospheric
10 circulation in the Community Atmosphere Model, version 3. J. Climate, 21, 1487–1499. 2008.

11 Rogelj, J. and Knutti, R.: Geosciences after Paris, Nat. Geosci., 9, 187–189, 2016.

12 Rossow, W. B. and Dueñas, E. N.: The International Satellite Cloud Climatology Project (ISCCP) web
13 site: an online resource for research, Bull. Amer. Meteor. Soc., 85, 167–172, doi:10.1175/BAMS-85-
14 2-167, 2004.

15 Rossow, W. B. and Schiffer, R. A.: Advances in understanding clouds from ISCCP, Bull. Amer.
16 Meteor. Soc., 80, 2261–2287, 1999.

17 Samset, B. H., G. Myhre, M. Schulz, Y. Balkanski, S. Bauer, T. K. Berntsen, H. Bian, N. Bellouin, T.
18 Diehl, R. C. Easter, S. J. Ghan, T. Iversen, S. Kinne, A. Kirkevåg, J.-F. Lamarque, G. Lin, X. Liu, J.
19 Penner, Ø. Seland, R. B. Skeie, P. Stier, T. Takemura, K. Tsigaridis, K. Zhang: Black carbon vertical
20 profiles strongly affect its radiative forcing uncertainty. Atmos. Chem. Phys., 13, 2423–2434,
21 doi:10.5194/acp-13-2423-2013, 2013.

22 Sand, M., Iversen, T., Bohlinger, P., Kirkevåg, A., Seierstad, I. A., Seland, Ø., and Sorteberg, A.: A
23 standardized global climate model study showing unique properties for the climate response to black
24 carbon aerosols. Accepted, Journal of Climate http://dx.doi.org/10.1175/JCLI-D-14-00050.1, 2015.

25 Sanderson, B. M., X. Yangyang, C. Tebaldi, M.Wehner, B. O'Neill, A. Jahn, A. G. Pendergrass, F.
26 Lehner, W. G. Strand, L. Lin, R. Knutti, and J. F. Lamarque: Community climate simulations to assess
27 avoided impacts in 1.5 and 2 _C futures. Earth Syst. Dynam., 8, 827–847, https://doi.org/10.5194/esd-
28 8-827-2017, 2017.

29 Schleussner C.-F., Rogelj, J., Schaeffer, M., Lissner, T., Licker, R., Fischer, E. M., Knutti, R.,
30 Levermann, A., Frieler, K., and Hare, W.: Science and policy characteristics of the Paris Agreement
31 temperature goal, Nat. Clim. Change, 6, 827–835, doi:10.1038/nclimate3096, 2016.

Earth System
Dynamics

Discussions

Open Access

EGU

1   Schwarz, J. P., J. R. Spackman, R. S. Gao, L. A. Watts, P. Stier, M. Schulz, S. M. Davis, S. C. Wofsy,

2   and D. W. Fahey: Global-scale black carbon profiles observed in the remote atmosphere and compared

3   to models, Geophys. Res. Lett., 37, L18812, doi:10.1029/2010GL044372, 2010

4   Schwarz, J. P., Samset, B. H., Perring, A. E., Spackman, J. R., Gao, R. S., Stier, P., Schulz, M.,

5   Moore, F. L., Ray, E. A., and Fahey, D. W.: Global-scale seasonally resolved black carbon vertical

6   profiles over the Pacific, Geophys. Res. Lett., 40, 5542–5547, doi:10.1002/2013gl057775, 2013.

7   Screen, J. A. and I. Simmonds: The central role of diminishing sea ice in recent Arctic temperature

8   amplification. *Nature* **464,** 1334–1337, 2010.

9   Seland, Ø. and Debernard, J. B., Sensitivities of Arctic Sea-ice in Climate Modelling, In: ACCESS

10   Newsletter. No. 9, 10-13, 2014. http://www.access-eu.org/en/publications/access_newsletter.html.

11   Seland, Ø., Iversen, T., Kirkevåg, A., and Storelvmo, T.: Aerosol-climate interactions in the CAM-

12   Oslo atmospheric GCM and investigations of associated shortcomings, Tellus, 60 A, 459-491, 2008.

13   Senior, C. A. and J. F. B. Mitchell: The time-dependence of climate sensitivity. Geophys. Res. Lett.,

14   27, 2685–2688. doi:10.1029/2000GL011373. 2000.

15   Seethala, C. and Horvath, A.: Global assessment of AMSRE and MODIS cloud liquid water path

16   retrievals in warm oceanic clouds, J. Geophys. Res., 115, D13202, doi:10.1029/2009JD012662, 2010.

17   Soden, B. J., I. M. Held, R. Colman, K. Shell, and J. T. Kiehl: Quantifying climate feedbacks using

18   radiative kernels. J. Climate, 21, 3504–3520, doi:10.1175/2007JCLI2110.1, 2008.

19   Spencer, R. W.: Global oceanic precipitation from the MSU during 1979–91 and comparisons to other

20   climatologies, J. Climate, 6, 1301–1326, 1993.

21   Stjern, C.W., B.H. Samset, G. Myhre, P.M. Forster, Ø. Hodnebrog, T. Andrews, O. Boucher, G.

22   Faluvegi, T. Iversen, M. Kasoar, V. Kharin, A. Kirkevåg, J.-F. Lamarque, D. Olivié, T. Richardson, D.

23   Shawki, D. Shindell, C.J. Smith, T. Takemura, A. Voulgarakis, F. Zwiers: Rapid adjustments cause

24   weak surface temperature response to increased black carbon concentrations., J. Geophys. Res., in

25   print.doi:10.1002/2017JD027326, 2017.

26   Straus, D. M. And J. Shukla: Does ENSO force the PNA? J. Clim., 15, 2340-2358. 2002.

27   Subramanian, A. C., M. Jochum, A. J. Miller, R. Murtugudde, R. B. Neale and D. E. Waliser: The

28   Madden Julian Oscillation in CCSM4. J. Climate, 24, 6261-6282. DOI: 10.1175/JCLI-D-11-00031.1.

29   2011.

30   Taylor, K. E., R. J. Stouffer, and G. A. Meehl: An overview of CMIP5 and the experiment design,

31   Bull. Am. Meteorol. Soc., 90, 485–498, doi:10.1175/BAMS-D-11-00094.1. 2012.

32   Tibaldi, S. and F. Molteni: On the operational predictability of blocking. Tellus, 42A, 343–365. 1990.

Earth System
Dynamics
Discussions

1   Trenberth, K.E.: The definition of El Niño. Bull Am Meteorol Soc, 78, 2771–2777. 1997.

2   Trenberth, K. E., J. T. Fasullo, And J. Mackaro: Atmospheric Moisture Transports from Ocean to
3   Land and Global Energy Flows in Reanalyses. J. Climate, 24, 4907-4924. DOI:
4   10.1175/2011JCLI4171.1, 2011b.

5   Uppala, S. M, Kållberg, P. W., Simmons, A. J., Andrae, U., Bechtold, V. D. C., Fiorino, M., Gibson, J.
6   K., Haseler, J., Hernandez, A., Kelly, G. A., Li, X., Onogi, K., Saarinen, S., Sokka, N., Allan, R. P.,
7   Andersson, E., Arpe, K., Balmaseda, M. A., Beljaars, A. C. M., Berg, L. V. D., Bidlot, J., Bormann,
8   N., Caires, S., Chevallier, F., Dethof, A., Dragosavac, M., Fisher, M., Fuentes, M., Hagemann, S.,
9   H´olm, E., Hoskins, B. J., Isaksen, L., Janssen, P. A. E. M., Jenne, R., Mcnally, A. P., Mahfouf, J. F.,
10 Morcrette, J. J., Rayner, N. A., Saunders, R. W., Simon, P., Sterl, A., Trenberth K. E., Untch, A.,
11 Vasiljevic, D., Viterbo, P., and Woollen, J.: The ERA-40 re-analysis. Q. J. Roy. Meteorol. Soc., 131,
12 2961-3012. 2005.

13 Yu L. and Weller, R. A.: Objectively analyzed air-sea heat fluxes for the global ice-free oceans (1981–
14 2005), Bull. Amer. Meteor. Soc., 88, 527–539, doi:10.1175/BAMS-88-4-527, 2007.

15 Yu, L., Jin, X., andWeller, R. A.: Multidecade Global Flux Datasets from the Objectively Analyzed
16 Air-sea Fluxes (OAFlux) Project: Latent and sensible heat fluxes, ocean evaporation, and related
17 surface meteorological variables, Tech. Rep. OA-2008-01, Woods Hole Oceanographic Institution,
18 Woods Hole, Massachusetts, USA, 2008.

19 van Vuuren, D. P., J. Edmonds, M. Kainuma, K. Riahi, A. Thomson, K. Hibbard, G. C. Hurtt, T.
20 Kram, V. Krey, J.-F. Lamarque, T. Masui, M. Meinshausen, N. Nakicenovic, S. J. Smith, and S. K.
21 Rose: The representative concentration pathways: an overview. Clim. Change, 109, 5–31. DOI:
22 10.1007/s10584-011-0148-z. 2011.

23 Wang, Y.-M., J. L. Lean, and N. R. Sheeley, Jr.: Modeling the Sun's magnetic field and irradiance
24 since 1713. Astrophys. J., 625, 522–538, 2005.

25 Williams, K.D., C.A. Senior, and Mitchell, J.F.: Transient Climate Change in the Hadley Centre
26 Models: The Role of Physical Processes. J. Climate, 14, 2659–2674, https://doi.org/10.1175/1520-
27 0442(2001)014<2659:TCCITH>2.0.CO;2, 2001.

28 Winton, M.: Amplified Arctic climate change: What does surface albedo feedback have to do with it?
29 Geophysical Research Letters, 33 (3), doi:10.1029/2005GL025244, 2006.

30 Zhang, C.: Madden–Julian oscillation, Rev. Geophys., 43, RG2003, doi:10.1029/2004RG000158,
31 2005.

Earth System
Dynamics
Discussions

1   Zhang, G. J. and McFarlane, N. A.: Sensitivity of climate simulations to the parameterization of
2   cumulus convection in the Canadian Climate Centre general circulation model. Atmos. Ocean 33,
3   407–446. 1995.

4

5

6

7

8

9

10

11

12

13

14

15

16

17

18

19

20

21

22

23

24

25

26

27

28   **Tables**

29

Earth System
Dynamics
Discussions

1   **Table 1**. Calculated global budgets for the on-line modelled aerosol components and precursors in an

2   AMIP experiment with NorESM1-Happi averaged over the 10 years 2006-2015 (Happi). The budget

3   is compared to an on-line run with NorESM1-M over the same years with RCP8.5-emissions for 2006-

4   2015 (M), and an off-line aerosol experiment with NorESM1-M valid for year 2000 (EmPD2000 in

5   Kirkevåg et al., 2013) (M_{2000}).

Comp.	NorESM1 version	Emis. Tg/a	Source Tg/a	Fraction of sink		Fraction of chem. loss 1: as MSA 2: in clear air %	Global burden Tg	Atmosph. residence time d
				as wet dep %	as chem. loss %			
DMS	Happi	18.0	18.0	0	100	27.0 (1)	0.12	2.43
	M	18.1	18.1	0	100	27.5(1)	0.12	2.38
	M_{2000}	18.0	18.0	0	100	27.1(1)	0.12	2.40
SO_2-S	Happi	64.7	78.1	8.4	67.7	16.1 (2)	0.25	1.16
	M	63.2	76.4	8.1	69.8	15.9 (2)	0.23	1.11
	M_{2000}	66.3	79.5	7.9	69.1	15.4 (2)	0.24	1.11
SO_4-S	Happi	1,66	54.6	92.3	0		0.55	3.68
	M	1.62	55.1	92.1	0		0.55	3.61
	M_{2000}	1.70	56.8	91.6	0		0.59	3.80
BC	Happi	8.58	8.58	78.1	0		0.14	5.73
	M	7.65	7.65	72.8	0		0.16	7.61
	M_{2000}	7.70	7.70	71.9	0		0.17	8.12
POM	Happi	123.6	138.2	80.4	0		2.38	6.24
	M	120.1	135.0	79.2	0		2.55	6.83
	M_{2000}	122.2	137.0	78.6	0		2.87	7.58
Sea-Salt	Happi	7397	7397	46.3	0		5.21	0.26
	M	6716	6716	47.7	0		4.81	0.26
	M_{2000}	6462	6462	45.4	0		4.94	0.28
Dust	Happi	1666	1666	24.6	0		12.10	2.64
	M	1674	1674	23.7	0		12.11	2.63
	M_{2000}	1672	1672	25.2	0		11.73	2.55

Earth System
Dynamics
Discussions

1   **Table 2.** Global and annual averages calculated for the two versions of the model (for 1976 - 2005 of

2   Hist1 for NorESM1-Happi and NorESM1-M) and for observationally based or reanalyzed data

3   (references below). The NorESM values are adjusted since the top of the model is slightly below the

4   TOA seen from satellites (Collins et al., 2006). The actual fluxes at the top of the model is shown in

5   Fig. 5, and the net radiative flux at the top of model for Hist1 (1976 – 2005) is about +0.61W m^{-2} in

6   NorESM1-Happi and +0.54W m^{-2} in NorESM1-M.

Variable (unit)	NorESM1-Happi 1 deg. resolution	NorESM1-M 2 deg. resolution	OBS / reanalysis
TOA net SW flux (W m^{-2})	240.2	234.9	240.6[a] 244.7[b] 234.0[c]
TOA net clear-sky SW flux (W m^{-2})	289.4	289.5	287.6[a] 294.7[b] 289.3[c]
TOA upward LW flux (W m^{-2})	237.6	232.4	239.6[a] 239.0[b] 233.9[c]
TOA clear-sky upward LW flux (W m^{-2})	263.5	262.3	266.1[a] 266.9[b] 264.4[c]
TOA LW cloud forcing (W m^{-2})	25.81	29.90	26.48[a] 27.19[b] 30.36[c]
TOA SW cloud forcing (W m^{-2})	-49.20	−54.57	−47.07[a] −48.59[b] −54.16[c]
Cloud cover (%)	46.36	53.76	66.80[d] 66.82[e]
Cloud liquid water path (g m^{-2})	121.3	125.3	112.6[f]
Surface sensible heat flux (W m^{-2})	18.0	17.8	19.4[h] 15.8[i] 13.2[j]
Surface latent heat flux (W m^{-2})	83.7	81.7	87.9[h] 84.9[k] 82.4[g] 89.1[l]

[a]CERES-EBAF (Loeb et al., 2005, 2009, 2012); [b]CERES (Loeb et al., 2005, 2009,2012), [c]ERBE (Harrison et al., 1990; Kiehl and Trenberth, 1997), [d]ISCCP (Rossow and Schiffer, 1999; Rossow and Dueñas, 2004), [e]CLOUDSAT (L'Ecuyer et al., 2008), [f]MODIS (Greenwald, 2009; Seethala and Horváth, 2010), [g]ERA40 (Uppala et al., 2005), [h]JRA25 (Onogi et al., 2007), [i]NCEP (Kanamitsu et al., 2002), [j]LARYA (Large and Yeager, 2004, 2008), [k]ECMWF (Trenberth et al., 2011), [l]WHOI (Yu and Weller, 2007; Yu et al., 2008).

7

8

Earth System
Dynamics
Discussions

1   **Table 3**. Bias and RMS error for selected atmospheric variables in the Hist1 (1976-2005) from

2   NorESM1-M and NorESM1-Happi. Obs. Data: Cloudsat (L'Ecuyer et al., 2008); CRU (Mitchell and

3   Jones, 2005; Morice et al., 2012); HadISST (Hurrel et al., 2008); GPCP, (Adler et al., 2003; Huffman

4   et al., 2009); ISCCP (Rossow and Schiffer, 1999; Rossow and Dueñas, 2004). Numbers are produced

5   by the diagnostic package from NCAR.

		Total cloud cover %		T_{2m} continents CRU K	SST HadISST K	Total Precip. GPCP mm d^{-1}
		Cloudsat	ISCCP			
Happi	bias	-20.46	-20.44	-1.45	-0.56	0.19
	rmse	22.08	23.01	2.40	1.19	1.15
M	bias	-13.06	-13.04	-0.88	-0.25	0.13
	rmse	15.64	17.40	2.38	1.24	1.22

6
7

1 **Table 4**. NH and SH sea-ice extent and standard deviation (both in 10^6 km^2) calculated for March and

2 September in the Hist1 runs with NorESM1-M and NorESM1-Happi and from observations (OSI-

3 SAF, 2017) for the years 1979–2005. The best estimate ice concentration fields from the observations

4 were interpolated to the model grid before the extents were calculated.

			Extent (10^6 km^2)	Std (10^6 km^2)	Deviation (10^6 km^2)
NH	March	OBS	15.41	0.42	0
		M	14.34	0.25	-1.09
		Happi	14.72	0.26	-0.69
	Sept.	OBS	6.9	0.62	0
		M	8.49	0.4	1.59
		Happi	7.95	0.40	1.05
SH	March	OBS	4.46	0.41	0
		M	5.65	0.46	1.19
		Happi	5.17	0.51	0.71
	Sept.	OBS	18.76	0.34	0
		M	19.25	0.50	0.49
		Happi	19.98	0.44	1.22

5

6 **Table 5**. Three estimates of equilibrium climate sensitivity (ECS) for abrupt doubling of atmospheric

7 CO_2 concentrations, two estimates of the overall feedback parameter, and two estimates of the

8 transient climate response (TCR) of NorESM1-Happi with 1° resolution, compared to NorESM1-M

9 with 2° resolution (Iversen et al, 2013), and for CCSM4 with 1° resolution (Bitz et al., 2012).

Model	ΔT_{eq} K	ΔT_{eff} K	ΔT_{reg} K	R_{f_reg} W m^{-2}	λ_{reg} W m^{-2} K^{-1}	λ_{eff} W m^{-2} K^{-1}	ΔT_{TCR} K	$\Delta T_{TCR,eff}$ K
CCSM4, 1 deg.	3.20	2.78	2.80	2.95	-1.053	-1.260	1.72	2.64
NorESM1-M 2 deg	3.50	2.86	2.86	3.17	-1.108	-1.224	1.37	2.29
NorESM1-Happi 1 deg	3.34	2,87	2.82	3.43	-1.214	-1.220	1.52	2.47

10

Earth System
Dynamics
Discussions

1 **Table 6**. Simulated changes in selected global annual data with NorESM1-Happi from the period

2 1976-2005 (Hist1) to 2071-2100 based on three projected representative concentration pathways

3 (RCP) scenarios. Column no. 3 from the right are total values simulated for 1976-2005 (Hist1) where

4 the water-cycle values can be compared to the budget values from Trenberth et al. (2011) in the

5 rightmost column. Column no. 2 from the right gives the differences between Hist1 (1976-2005) and

6 the 1850 piControl.

	RCP8.5 – Hist1	RCP4.5 – Hist1	RCP2.6 – Hist1	Hist1 1976-2005	Hist1 – piControl	Water Budget 2001-2008
T_{2m} (K)	+3.09	+1.59	+0.91	286.44	+0.55	-
SST (K)	+2.02	+1.03	+0.59	290.88	+0.36	-
$AREA_{SeaIce} (10^6 \, km^2)$	-6.6	-2.8	-1.7	20.7	-1.0	-
P_{GLOBAL} 1000 $km^3 \, yr^{-1}$	+28.1	+17.5	+11.9	533.5	+1.5	500
E_{OCEANS} 1000 $km^3 \, yr^{-1}$	+26.1	+15.1	+10.1	451.7	+1.3	426
$(E-P)_{OCEANS}$ 1000 $km^3 \, yr^{-1}$	+7.5	+3.3	+1.2	45.2	+0.6	40
P_{OCEANS} 1000 $km^3 \, yr^{-1}$	+18.2	+11.8	+8.9	406.5	+0.7	386
P_{LAND} 1000 $km^3 \, yr^{-1}$	+9.9	+5.7	+3.0	127.0	+0.8	114
E_{LAND} 1000 $km^3 yr^{-1}$	+2.5	+2.4	+1.8	81.8	+0.2	74

7

8

Earth System
Dynamics
Discussions

1   **Table 7**. NH and SH Polar Amplification Factor (PAF= $\Delta T_{Polar}/\Delta T_{Global}$, polar is the poleward side

2   of the 60° latitude) and the global temperature at reference height (2m) are listed for PD (2006-2015)

3   together with their increments for a 1.5 °C and a 2.0 °C warmer world than the 1850 pre-industrial.

4   Results are taken from the NorESM1-Happi AMIP-type runs and the NorESM1-HappiSO. Similar

5   results from the RCP2.6 and RCP4.5 projections at 2071-2100 with NorESM1-Happi compared to

6   Hist1 (1976-2005) are included for reference.

	Period or Difference	NH_PAF	SH_PAF	T_{2m} K
NorESM1-Happi AMIP 100x10 years	PD			287.30
	1.5 - PD	2.34	1.62	+0.71
	2.0 - PD	2.17	1.35	+1.20
	2.0 – 1.5	1.93	0.95	+0.49
NorESM1-Happi Slab Ocean 265 years	PD			287.17
	1.5 - PD	2.49	1.79	+0.68
	2.0 - PD	2.41	1.60	+1.19
	2.0 – 1.5	2.27	1.30	+0.51
NorESM1-Happi Coupled 30 years	Hist1			286.44
	RCP2.6 – Hist1	3.00	0.29	+0.91
	RCP4.5 – Hist1	2.70	0.58	+1.59
	RCP4.5 – RCP2.6	2.29	0.97	+0.68

7

1   **Table 8**. Similar as Table 7, but for 2m temperature over land, precipitation on land, and sea-ice area

2   in the northern, extratropical hemisphere (20-90 °N) in winter (DJF) and summer (JJA).

	Period or Difference	T_{Land}^{DJF} K	T_{Land}^{JJA} K	P_{Land}^{DJF} mm d^{-1}	P_{Land}^{JJA} mm d^{-1}	$AREA_{SeaIce}^{DJF}$ 10^6 km^2	$AREA_{SeaIce}^{JJA}$ 10^6 km^2
NorESM1-Happi AMIP 100x10 years	PD	264.89	293.60	1.212	2.538	11.90	6.31
	1.5 - PD	+1.43	+0.81	+0.067	+0.09	-0.99	-0.56
	2.0 - PD	+2.33	+1.66	+0.093	+0.13	-1.39	-0.89
	2.0 – 1.5	+0.90	+0.84	+0.026	+0.04	-0.40	-0.33
NorESM1-Happi Slab Ocean 265 years	PD	264.13	293.42	1.214	2.549	13.33	6.26
	1.5 - PD	+1.40	+1.24	+0.041	+0.054	-0.51	-0.34
	2.0 - PD	+2.24	+2.00	+0.063	+0.073	-0.75	-1.18
	2.0 – 1.5	+0.85	+0.77	+0.022	+0.019	-0.24	-0.84
NorESM1-Happi Coupled 30 years	Hist1	263.84	291.50	1.241	2.342	13.61	8.511
	RCP2.6 – Hist1	+1.98	+1.63	+0.047	+0.109	-1.56	-1.77
	RCP4.5 – Hist1	+3.19	+2.85	+0.072	+0.127	-2.29	-2.70
	RCP4.5 – RCP2.6	+1.21	+1.22	+0.025	+0.018	-0.73	-0.93

3

4

5

6

7

8

9

10

11

12

13

14

1   **Figures**

BC mixing ratio
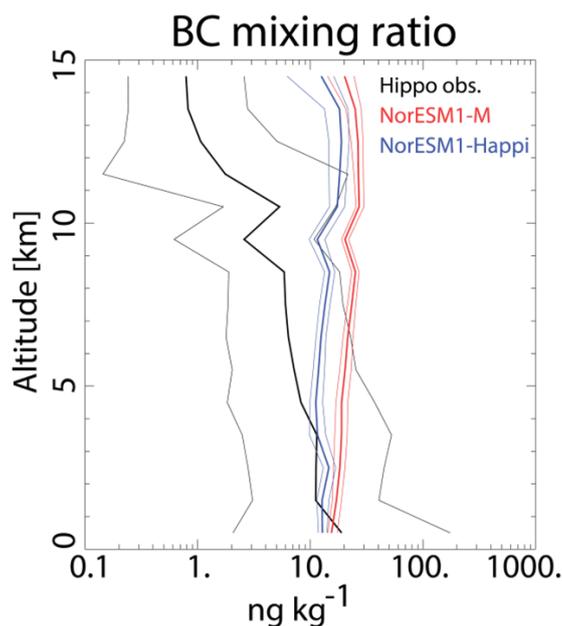
2

3   **Figure 1**. The modeled vertical profile of black carbon (BC) aerosols for AMIP-runs for PD (2006-

4   2015) with NorESM1-Happi (blue) and the fully coupled runs using RCP8.6 for the same period with

5   NorESM1-M (red). Thin lines indicate the inter-annual spread. Black lines are median (thick) and

6   ranges (thin) based on observations from the HIPPO campaign, with more than 700 vertical profiles

7   during 2009-2011 from 0.3 to 14 km altitude, mainly over the Pacific Ocean between 80ºN and 67ºS

8   (Schwartz et al., 2010 and 2013).

9
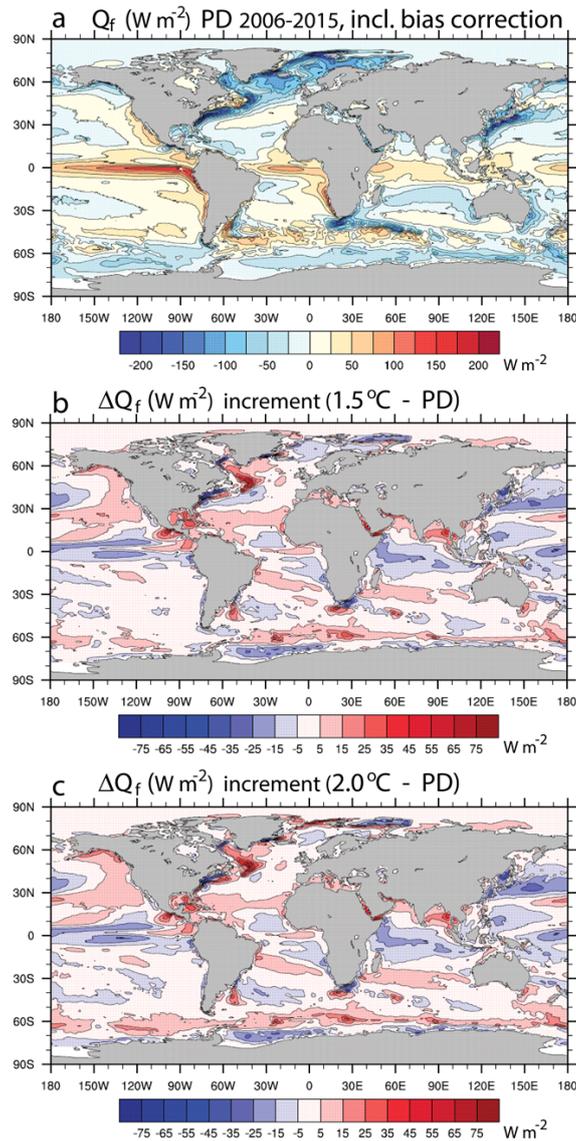
Figure 2. The annual average ocean net heat-flux Q_f calibrated for the slab ocean model, NorESM1-HappiSO to maintain a stable climate with a present-day, 2006-2015 (PD), observed SST-field under vanishing TOA net heat-flux (a). The change in Q_f from PD to a 1.5°C world (b) and from PD to a 2.0°C world (c), ensuring that the NorESM1-HappiSO produces a stable global climate comparable to the HAPPI AMIP runs with NorESM1-Happi without precribing the SSTs. Unit: W m^{-2}, negative values contribute to increasing SST (Eq. 1). The global averages are -1.32 W m^{-2} (PD), -1.94 W m^{-2} (1.5°C), and -1.71 W m^{-2} (2.0°C).

Earth System
Dynamics
Discussions
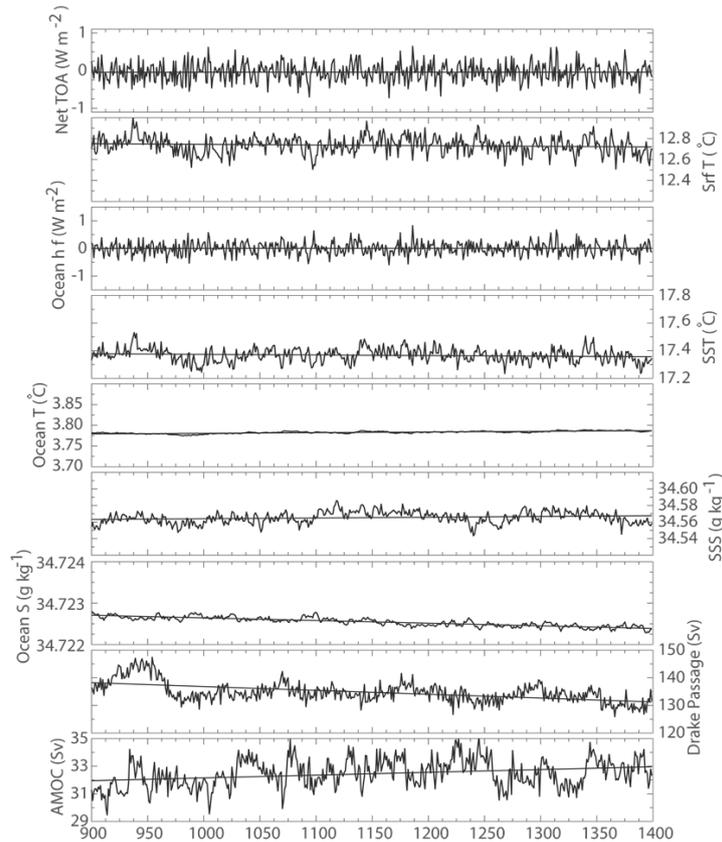
Figure 3. Annual mean time series between years 900 and 1400 from NorESM1-Happi piControl of, from top, net radiation at the Top of the Model Atmosphere, TOA, with positive values indicating warming of the atmosphere (mean value is -0.042 W m^{-2}); near surface air temperature (mean value is 12.74°C); net heat flux into the ocean/sea (positive value means ocean warming, mean value is +0.004 Wm^{-2}); SST (mean value is 17.37°C); volume-averaged ocean temperature (mean value is 3.78°C); SSS (mean value is 34.57 g kg^{-1}); volume-averaged ocean salinity (mean value is 34.72 g kg^{-1}), net volume transport through the Drake Passage (mean value is 135 Sv), and the strength of AMOC at 26.5°N (mean value is 32.4 Sv). The black dashed lines in the two heat flux panels show the zero value, whereas the solid black lines in the other panels show the linear trends for years 900–1400. The figure can be compared with Fig. 2 in Bentsen at el. (2013), except that the mean value of the TOA net radiation in that paper should be corrected to +0.043 W m^{-2}.

Earth System
Dynamics
Discussions

Open Access

1
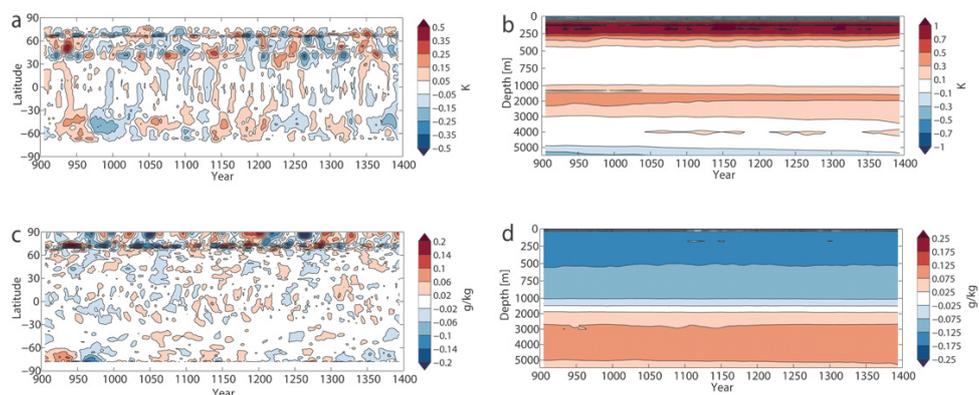
Figure 4. Latitude–time Hovmöller diagrams of (a) annual, zonal mean SST (K) and (c) SSS (g kg^{-1})
where the corresponding zonal time means have been subtracted, and depth–time Hovmöller diagrams
of (b) global mean ocean potential temperature (K) and (d) salinity (g kg^{-1}) presented as anomalies
compared to World Ocean Atlas 2009 (WOA09; Locarnini et al., 2010; Antonov et al., 2010) annual
mean potential temperature and salinity. All panels are based on years 900–1400 of NorESM1-Happi
piControl, filtered with a 10-year running mean. Note the non-linear depth co-ordinate in (b) and (d).

1
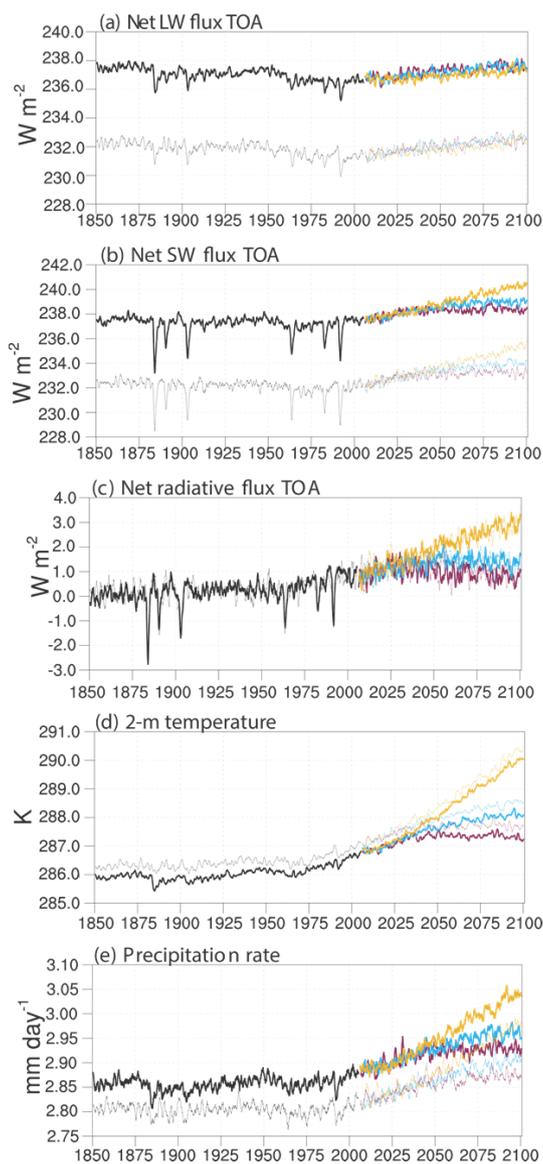
Figure 5. From the top panel and downwards, the figure shows the net global long-wave (positive upwards), short-wave (positive downwards), and total (positive downwards) radiative flux at the top of the model atmosphere (TOA) during the NorESM1-Happi coupled simulations for 1850 to 2100. The next two panels show diagrams for the global air temperature at reference height (2m) and monthly averaged precipitation rate. Black: Hist1; green: RCP2.6; blue: RCP4.5; red: RCP8.5. The curves for NorESM1-M (Iversen et al. 2013) are included as thinner lines for comparison.

1
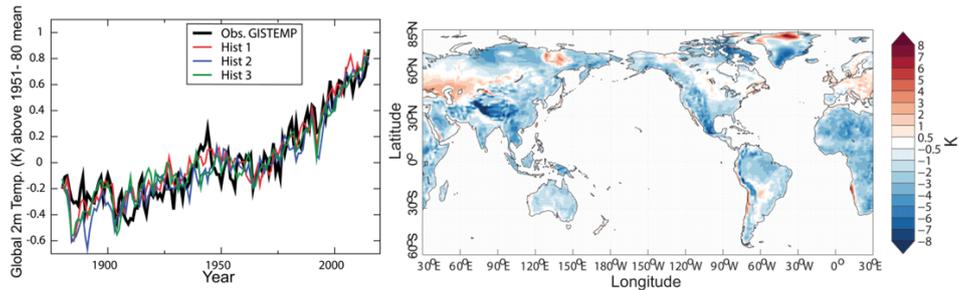
Figure 6. NorESM1-Happi global reference height air temperature compared with the NASA GISS global temperature record (Hansen et al., 2010) over the historical period 1850-2015 (left), and comparison of the reference height temperatures over continents for 1976-2005 with the CRU TS3.1 (Mitchell and Jones, 2005) observational data for the same period (right). Global bias is -1.45 K with a RMSE of 2.40 K (compared to -0.88 K and 2.38 K for NorESM1-M, see Table 3). In (a), three model-calculated ensemble members are presented, while in (b) only the first ensemble member is shown.

8
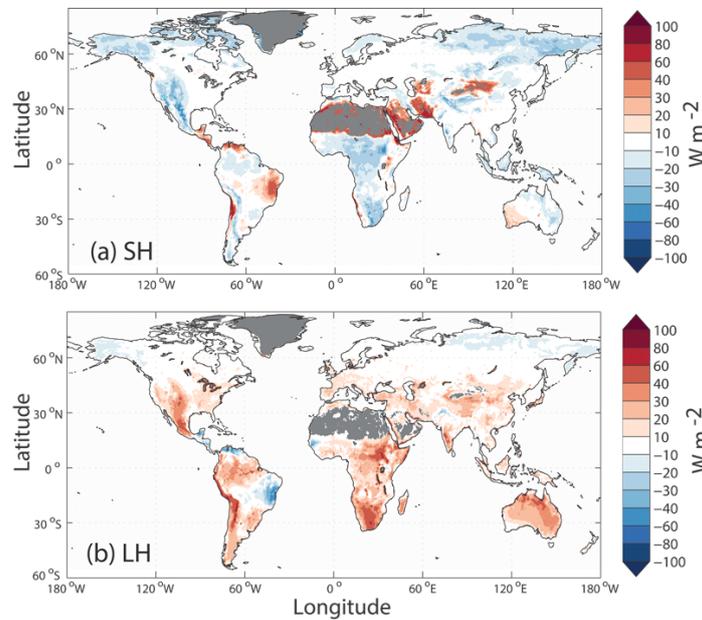
Figure 7. The difference between NorESM1-Happi and FLUXNET-MTE (Jung et al., 2011) fluxes of sensible heat (a) and latent heat (b). The NorESM1-Happi fluxes are means for the years 1976–2005 of the Hist1 experiment, and the FLUXNET-MTE fluxes are means for the years 1982–2005. Areas with missing observations are shaded with dark grey colour.

1
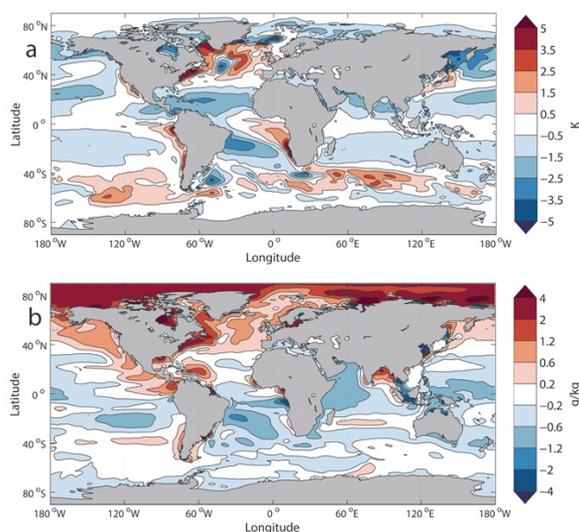
Figure 8. Differences between model calculated fields and observation-based data sets for SST (K) (a)

and SSS (g kg^{-1}) obtained from WOA09 (Locarnini et al., 2010; Antonov et al., 2010).

4
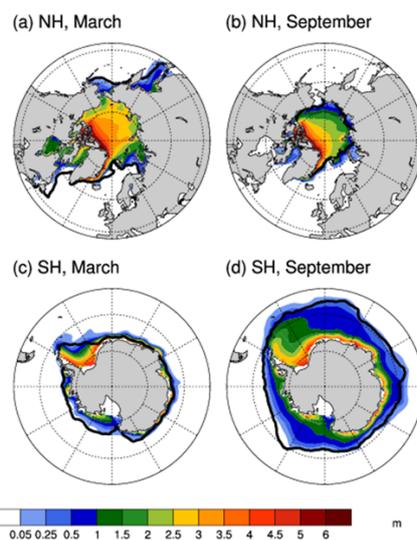
Figure 9. Mean sea-ice thickness (m) over years 1976–2005 of the NorESM1-Happi Hist1 experiment

for both hemispheres and for (a, c) March and (b, d) September. The solid black line shows the 15%

monthly sea ice concentration from the OSI-SAF reprocessed data set (OSI-SAF, 2017).
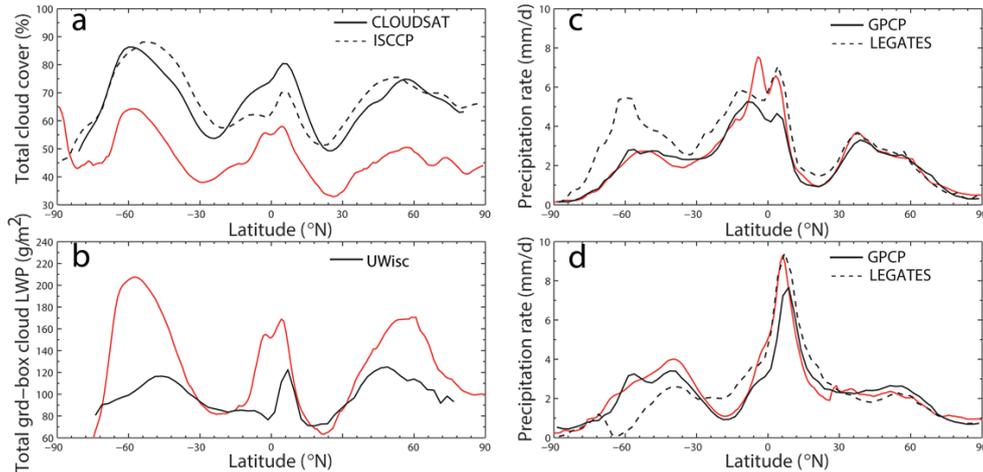
Figure 10. (a) Zonally averaged total cloud fraction (%) of NorESM1-Happi compared to ISCCP D2-retrievals 1983–2001(Rossow and Schiffer, 1999; Rossow and Dueñas, 2004) and Cloudsat radar and lidar retrievals from September 2006 – December 2010 (L'Ecuyer et al., 2008). **(b)** Zonally averaged total liquid water path (g m^{-2}) of NorESM1-Happi compared to UWisc retrievals over oceans for the period 1988–2008 (O'Dell et al., 2008). **(c)** Zonally averaged boreal winter (DJF) estimated annual precipitation of NorESM1-Happi compared to the data from GPCP (Adler et al., 2003) and Legates (Spencer, 1993; Legates and Willmott, 1990), and **(d)** the same for boreal summer (JJA). NorESM1-Happi values shown in red are means for the years 1976–2005 of the Hist1 experiment.
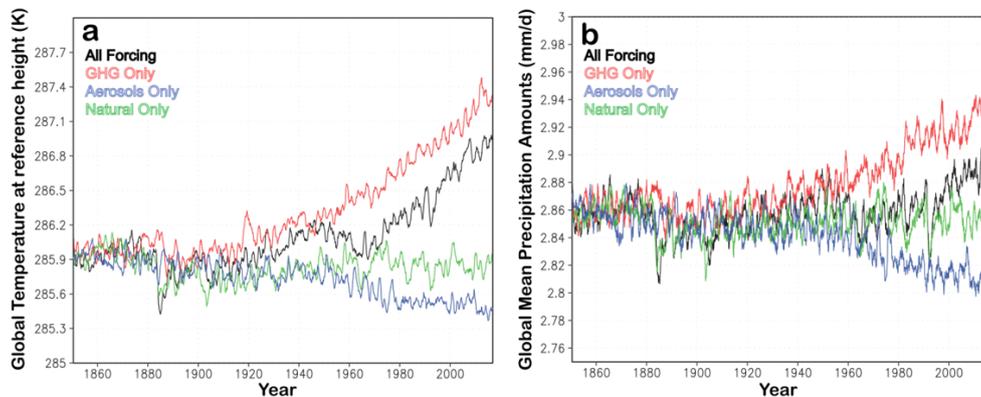
Figure 11. NorESM1-Happi global reference height air temperatures (a) and global mean diurnal precipitation amounts (b) over the historical period 1850-2015 for all and selected single forcings as well as the total forcing experiments for Hist1.

1

2

3
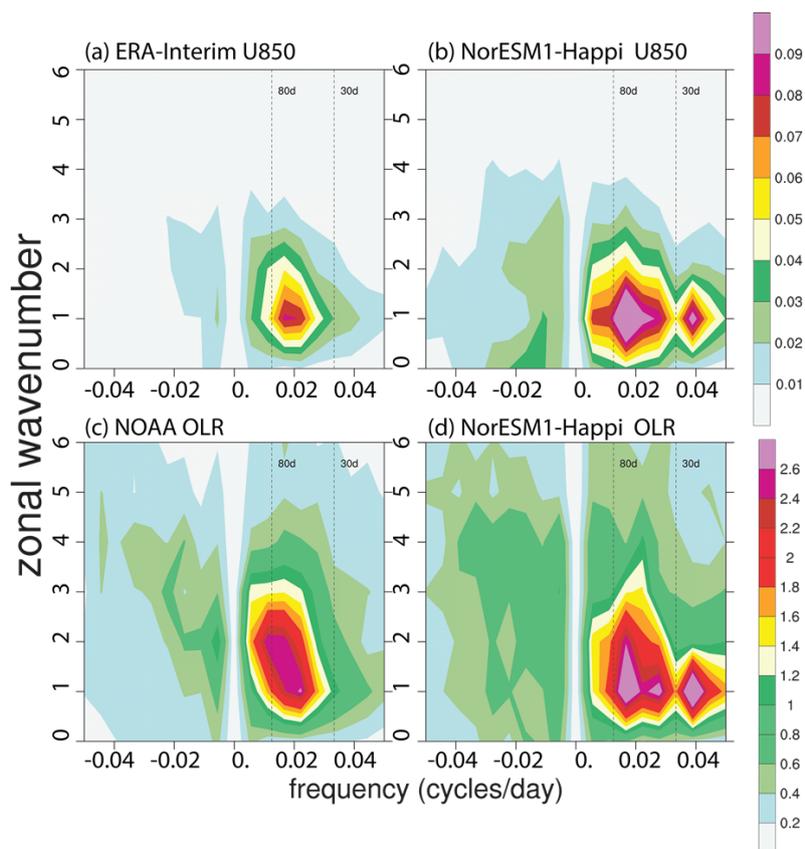
Figure 12. November–April wavenumber–frequency spectra of 10° S – 10° N averaged daily zonal 850 hPa winds of (a) ERA-Interim (1979–2008) (Dee et al., 2011) and (b) NorESM1-Happi (1976–2005), and daily outgoing long-wave radiation (OLR) of (c) NOAA satellite (1979–2008) and (d) NorESM1-Happi (1976–2005). Individual spectra were calculated for each year and then averaged over all years of data. Only the climatological seasonal cycle and time-mean for each November–April segment were removed before calculation of the spectra. Units for the zonal wind (OLR) are m^{-2} s^{-2} (W m^2 s^{-1}) per frequency interval per wavenumber interval. The band-width is 180 day^{-1}.

11

1
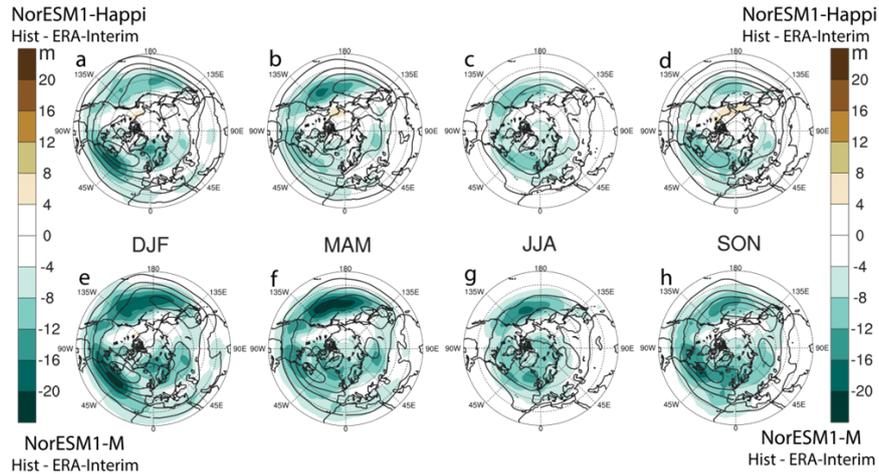
Figure 13. Estimated seasonal biases (coloured, unit m) of the NH extra-tropical cyclone activity, calculated as the standard deviation of the band-pass time-filtered geopotential height at 500hPa in the Hist ensembles (1976-2005) from NorESM1-Happi (a-d) and NorESM1-M (e-h) relative to the cyclone activity from ERA-Interim (1979-2008, Dee et al., 2011). Continuous lines show the Hist cyclone activity for the respective model. Cyclone activity is estimated by applying a 2.5 - 6 days band-pass time filter to the 500 hPa geopotential height before taking the standard deviation.

8
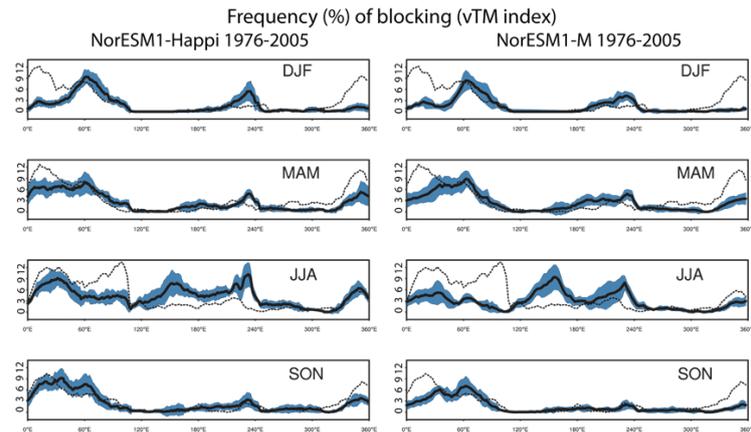
Figure 14. NH blocking frequency (%) for three Hist ensemble-members for NorESM1-Happi (left) and NorESM1-M (right) over the years 1976-2005 are presented. The solid black curves represent the ensemble mean, the blue shading is the ensemble spread (one standard deviation), and the dotted black curves are for the ERA-Interim data 1979-2008 (Dee et al., 2011). The seasonal occurrence of blocking is based on the 500 hPa vTM-index (Tibaldi and Molteni, 1990) relative to the latitudes of the average position of the westerlies by season (Pelly and Hoskins, 2002).

Earth System
Dynamics
Discussions

1
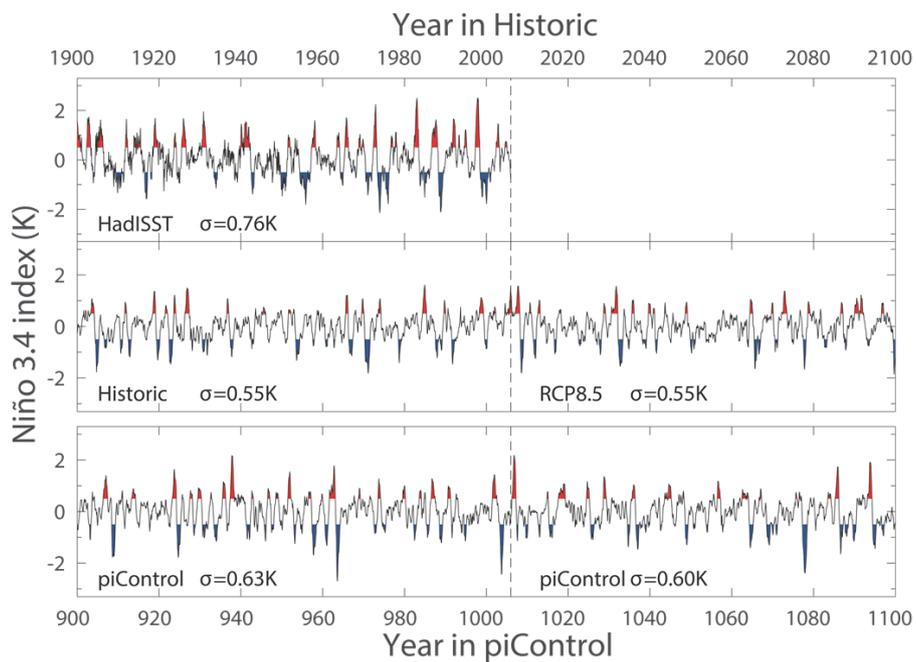
Figure 15. The time series of de-trended monthly SST anomalies of the NINO3.4 region (5°S-5°N; 170°W-120°W). The anomalies are found by subtracting the monthly means for the whole time series. Red (blue) colours indicate that anomalies are larger (smaller) than +0.4 K (-0.4 K), see Trenberth (1997) for recommendations. The upper time series shows Hadley Centre Sea Ice and SST data set (HadISST; Rayner et al., 2003) for years 1900-2005; the middle time series consist of NorESM1-Happi Hist1 for years 1900-2005 continued with NorESM1-M RCP8.5 for years 2006-2100; and the lower time series displays NorESM1-Happi piControl for years 900-1100.

10

11

12

13

1
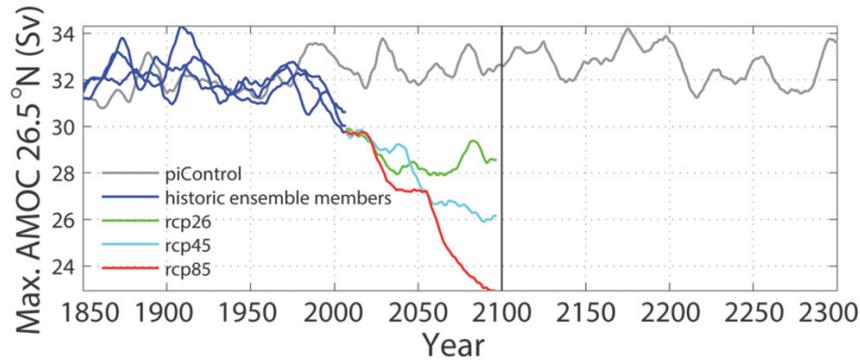
Figure 16. Decadal moving averages of the annual max AMOC at 26.5°N from the NorESM1-Happi simulations for 1850 to 2100 are presented. Black represents the piControl, blue the 1850-2005 Hist1, 2 and 3; green the RCP2.6, turquoise the RCP4.5, and red the RCP8.5 projections over 2005-2100. The grey curve is from the piControl
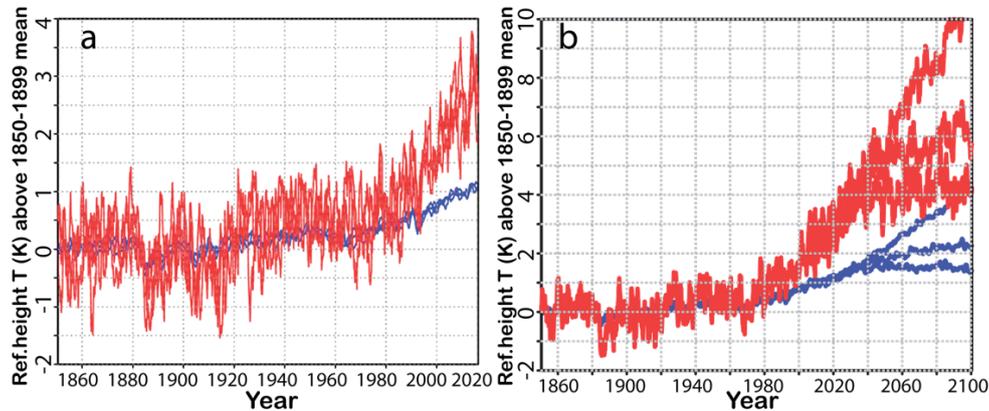

Figure 17. Simulated development in temperature at reference height with NorESM1-Happi relative to the 1850–1899 average for the globe (red) north of 65° N (blue), i.e. ca. 4.7% of the global area. Three historical ensemble members from 1850 to 2005 extended to 2015 with RCP8.5 are shown in (a), and Hist1 until 2005 followed by a range defined by the three RCP scenario projections up to 2100 are shown in (b).
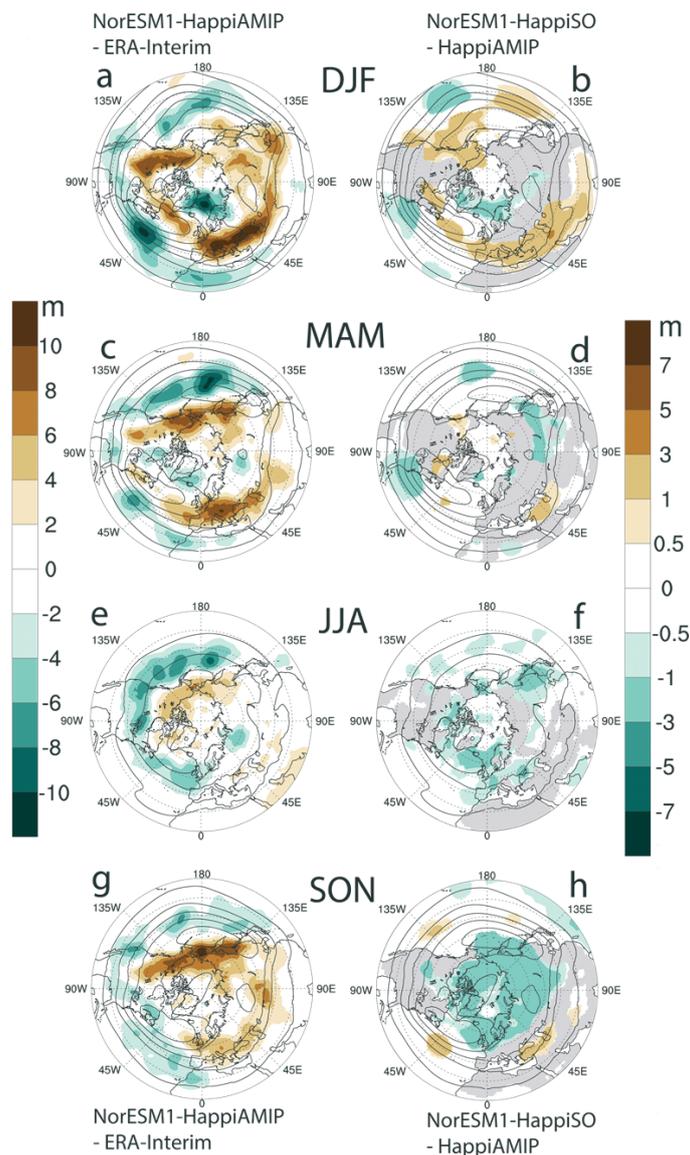
Figure 18. NH extra-tropical cyclone activity for PD (2006-2015). Seasonal results from the AMIP-ensemble for HAPPI with the NorESM1-Happi model compared to ERA-Interim data for the same decade (Dee et al., 2011) are shown as coloured shadings in a, c, e, and g. Differences between the results of the slab-ocean runs with NorESM1-HappiSO and the AMIP-ensemble are shown for each season as coloured shadings in b, d, f, and h. The black iso-lines are the diagnosed cyclone activity in the AMIP-ensemble (left) and SO ensemble (right) for each season. The shadings are shown where differences are statistically significant at the 5% level according to the Welch t-test.
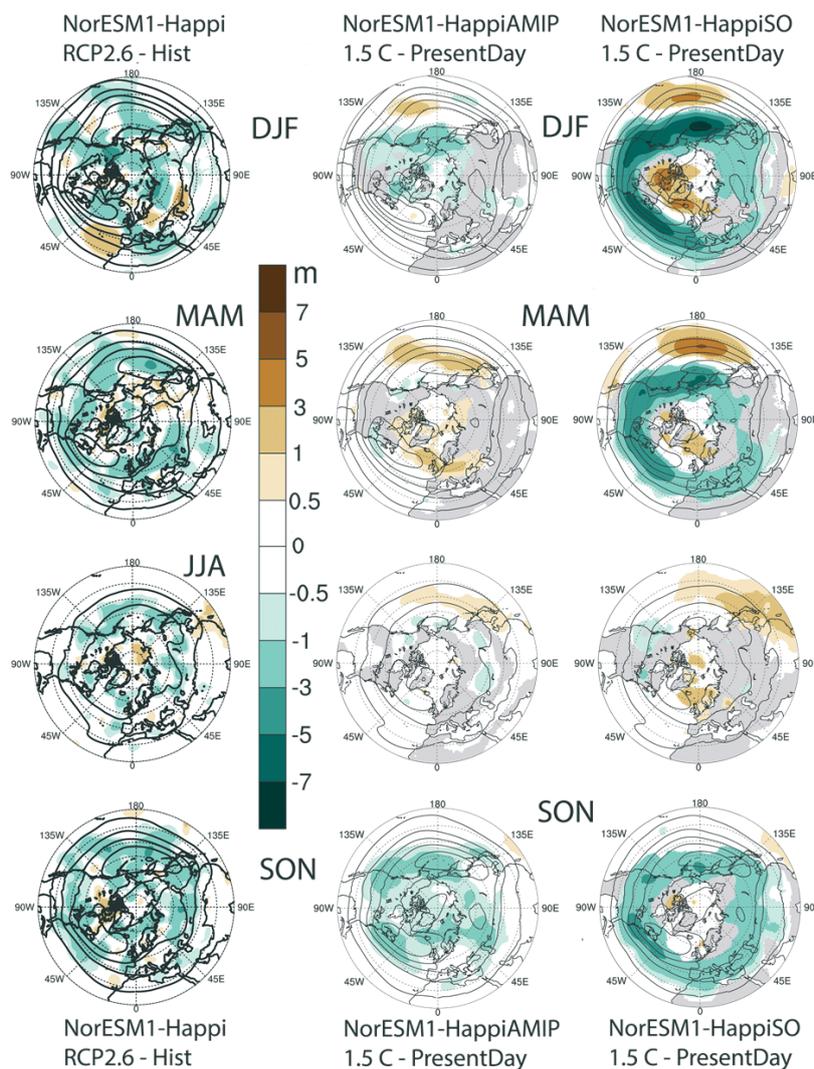
**Figure 19**. Coloured shadings show changes in the seasonal NH extra-tropical cyclone activity from the Hist (1976-2005) to the RCP2.6 projection (2071-2100) with NorESM1-Happi (left column), and from PD (2006-2015) to a 1.5°C warmer world estimated by the AMIP-ensemble from NorESM1-Happi (middle column) and the slab ocean experiment with NorESM1-HappiSO (right column). The black iso-lines are the diagnosed cyclone activity for Hist (left) or PD (middle and right) estimated from the respective model simulations for each season. The shadings are shown where the differences are statistically significant at the 5% level according to the Welch t-test.
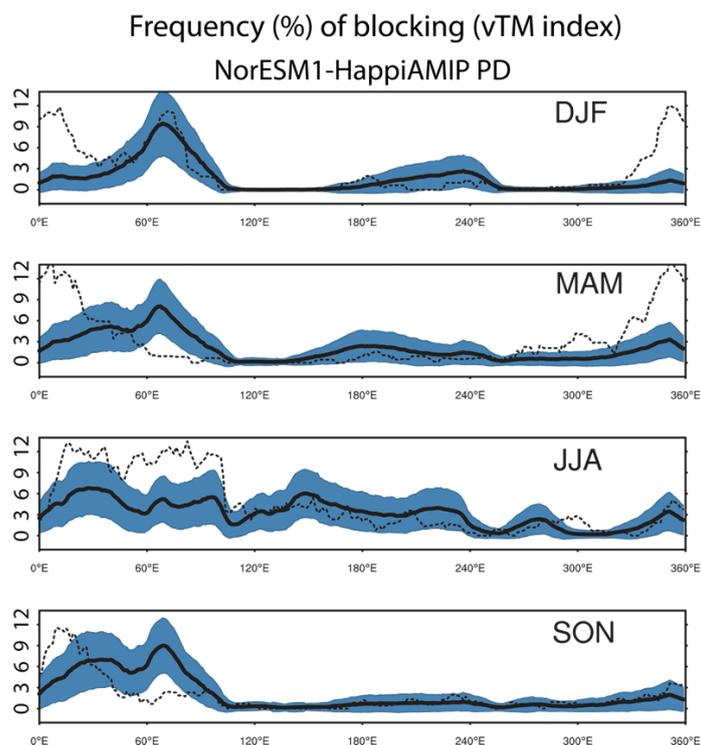
Figure 20. Blocking frequency of occurrence for the ensemble of NorESM1-Happi AMIP runs for PD (2006-2015). The solid black curve is the ensemble mean, while the blue shading shows the standard deviation in the ensemble of 10-year long runs around the ensemble mean. The dashed black lines show results for ERA-Interim over the same decade. Results for the 265 years with the NorESM1-HappiSO are almost identical to the results shown for the NorESM1-Happi AMIP runs.
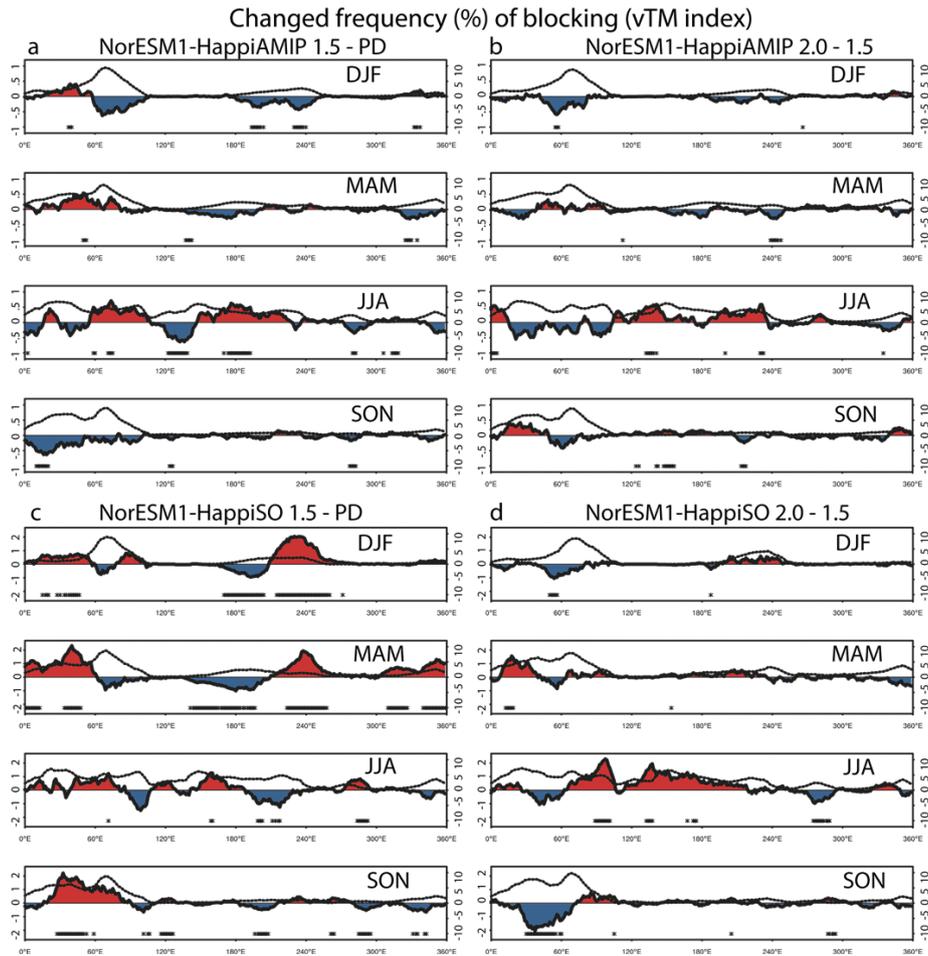
Figure 21. (a) Change in blocking frequency for the NorESM1-Happi AMIP ensemble experiment for a 1.5 °C world compared to PD 2006-2015. The solid black line shows the ensemble mean difference with blue shading indicating reduced blocking occurrence and red indicating increased. The dashed black line shows the estimated PD climatology for reference. (b) Change in blocking frequency for NorESM1-HappiAMIP ensemble for an additional 0.5°C global warming. The solid black line shows the ensemble mean difference between the 2.0°C and the 1.5°C experiment, with blue and red shading to indicate reduced and increased occurrence respectively. The dashed black line shows the 1.5°C experiment climatology for reference. The diagrams (c) and (d) are similar results for the slab-ocean model NorESM1-HappiSO. Dots mark differences that are statistically significant at the 5% level according to the Welch t-test. *Note*: the y-axis to the left is for the colored difference, while that to the right is for the climatological occurrence curves.

1
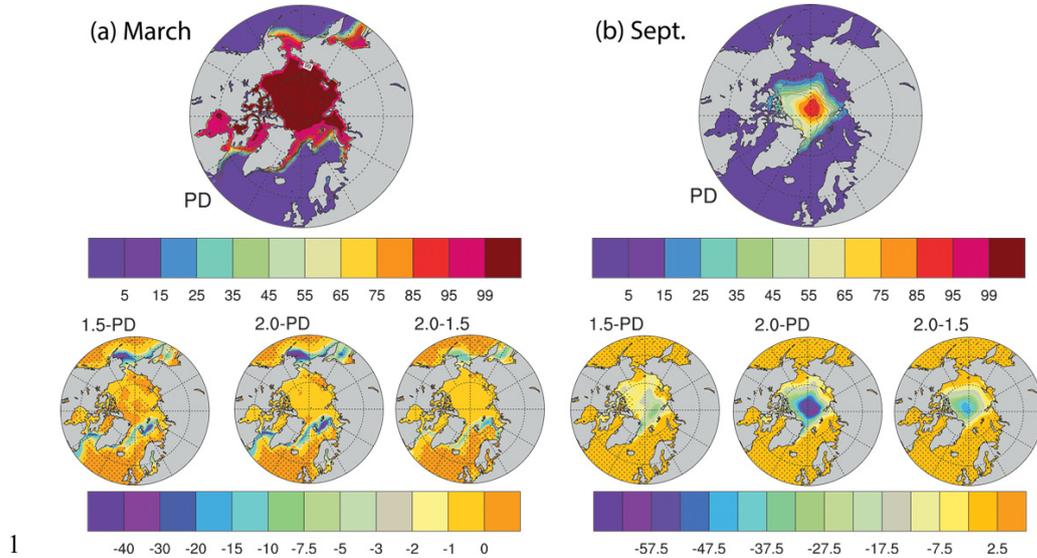
Figure 22. Calculated NH ice-concentrations (% of grid square area) for March (a) and September (b) in the NorESM1-HappiSO model averaged over 265 years after 45 years of spin-up. PD are results for 2006-2015 together with observational estimates shown as solid black lines (OSI-SAF, 2017). Increments in the ice-concentrations from PD to a 1.5°C warmer and a 2.0°C warmer world respectively, and for the difference between the latter, are shown below. Differences are not significant on the 5% level in areas marked with dots, according to the Mann-Whitney U test assuming that different decades are un-correlated.
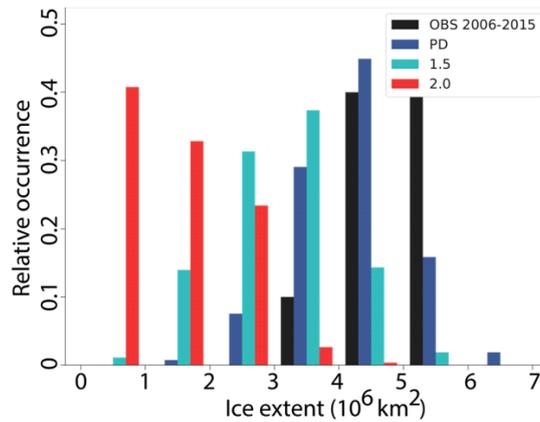
Figure 23. The relative occurrence of NH sea-ice extent counted in classes of width $1.\times10^6$ km^2 are presented for the simulated PD climate with NorESM1-HappiSO (blue columns), to be compared with observations (black columns; OSI-SAF, 2017), the 1.5°C warmer (turquoise columns), and the 2.0°C warmer world (red columns) relative to the 1850 pre-industrial climate.